NASA Environmentally Responsible Aviation Hybrid Wing Body Flow-Through Nacelle Wind Tunnel CFD

Michael J. Schuh[1] and Joseph A. Garcia[2]
NASA Ames Research Center, Moffett Field, CA, 94035, USA

Melissa B. Carter[3] and Karen A. Deere[3]
NASA Langley Research Center, Hampton VA, 23681, USA

Paul M. Stremel[4]
Science and Technology Corporation, NASA Research Park, CA, 94035, USA

and

Daniel M. Tompkins[5]
Boeing Research & Technology, Huntington Beach, CA, 92647, USA

Wind tunnel tests of a 5.75% scale model of the Boeing Hybrid Wing Body (HWB) configuration were conducted in the NASA Langley Research Center (LaRC) 14'x22' and NASA Ames Research Center (ARC) 40'x80' low speed wind tunnels as part of the NASA Environmentally Responsible Aviation (ERA) Project. Computational fluid dynamics (CFD) simulations of the flow-through nacelle (FTN) configuration of this model were performed before and after the testing. This paper presents a summary of the experimental and CFD results for the model in the cruise and landing configurations.

Nomenclature

α	=	Angle of Attack
C_D	=	drag coefficient
C_L	=	lift coefficient
C_M	=	moment coefficient
y^+	=	nondimensional first cell height

Acronyms

ARC	=	Ames Research Center
CFD	=	computational fluid dynamics
ERA	=	Environmentally Responsible Aviation
FTN	=	flow-through nacelle
HWB	=	hybrid wing body
LaRC	=	Langley Research Center
NASA	=	National Aeronautics and Space Administration
RANS	=	Reynolds-averaged Navier-Stokes
SA	=	Spalart-Allmaras
SST	=	shear stress transport

[1] Aerospace Engineer, System Analysis Office, Aeronautics Directorate, Mail Stop 258-1.
[2] Aerospace Engineer, System Analysis Office, Aeronautics Directorate, Mail Stop 258-1, AIAA Senior Member.
[3] Aerospace Engineer, Configuration Aerodynamics Branch, Mail Stop 499, AIAA Senior Member.
[4] Senior Research Scientist, Mail Stop 258-1, AIAA Member.
[5] Propulsion Engineer, Flight & Vehicle Technology, Boeing Research & Technology, AIAA Senior Member.

I. Introduction

NASA's Environmentally Responsible Aviation (ERA) Project explores enabling technologies to reduce aviation's impact on the environment. One research challenge area for the project has been studying advanced airframe and engine integration concepts to reduce community noise and fuel burn. In order to achieve this, wind tunnel tests at both the NASA LaRC 14'x22' and the NASA ARC 40'x80' low speed wind tunnels have been conducted on a 5.75% scale model of the Boeing Hybrid Wing Body (HWB) 0009GM[1] configuration. These wind tunnel tests entailed various entries to evaluate the propulsion airframe interference including aerodynamic performance and aeroacoustics. In order to baseline the powered configurations being tested, a simplified engine modeled as a flow-through nacelle (FTN) configuration was tested as well. This paper provides a summary of CFD simulations from four different flow solvers that were conducted in advance of the FTN test in support of model integration hardware design as well as some post-test aerodynamic performance data comparisons. Figure 1 shows computed pressure coefficients contours on the HWB in the 40'x80' wind tunnel.

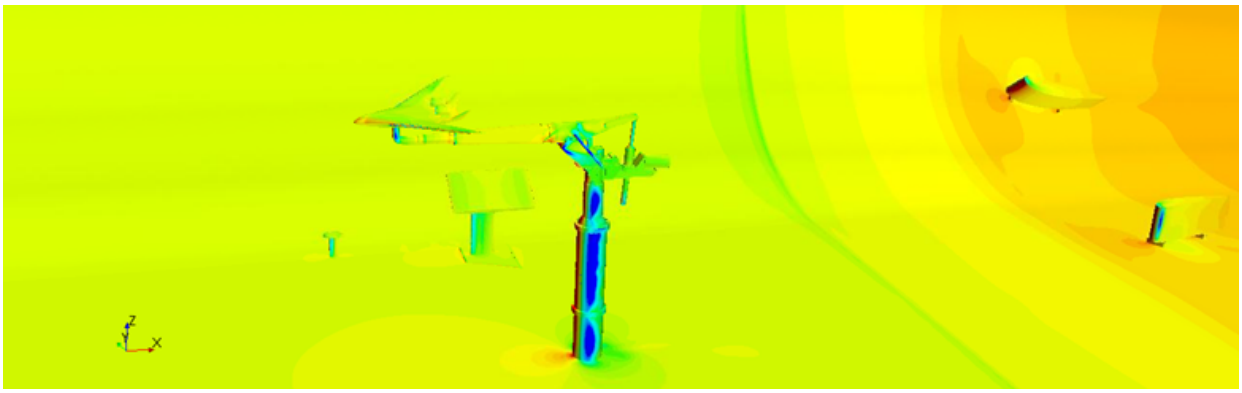

Figure 1. CFD solution within the ARC 40'x80' wind tunnel facility.

Figure 2 shows a configuration of the ERA HWB model tested in the wind tunnels. CFD simulations were performed in the months prior to testing. The HWB model was tested in the 14'x22' wind tunnel during July of 2014. It was tested in the 40'x80' wind tunnel during January and February of 2015 and again during June to August of 2015. Data were collected for the model in the FTN configuration during each of these test periods.

This paper presents simulation results for four different CFD codes, CFD++, OVERFLOW, STAR-CCM+, and USM3D and the wind tunnel test data for the FTN model in both the landing and cruise configurations. CFD predictions were made for the model in free air, free air with the wind tunnel sting, and in the wind tunnels with the sting, vertical support structures and walls.

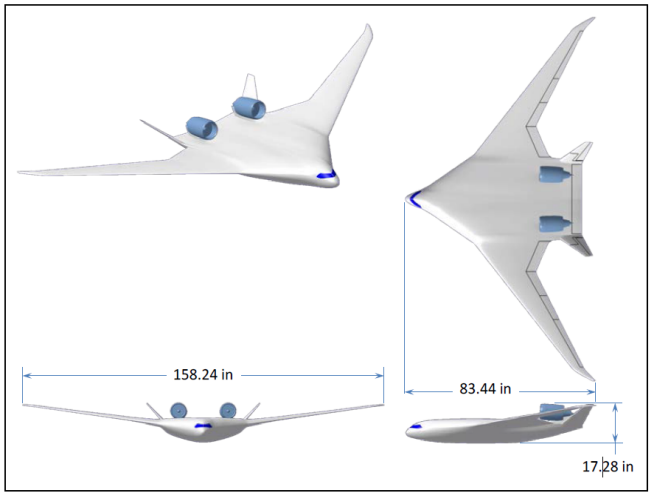

Figure 2. HWB vehicle.

II. CFD Codes

Four codes were used to simulate various configurations of the HWB vehicle. The HWB cruise and landing configurations were simulated in free air and in the two wind tunnels. The free air simulations were made without and with the wind tunnel sting. The descriptions of the four CFD codes used in this effort are presented next followed by comparisons of the CFD simulation results with the 14'x22' and 40'x80' wind tunnel measurements.

CFD++ was used by Boeing to perform Reynolds-averaged Navier-Stokes (RANS) simulations on unstructured grids. CFD++ is available from Metacomp Technologies[2]. The primary turbulence model employed was the two-equation realizable k-epsilon model. The grids were created with the Pointwise[3] software. The local grid spacing

was set to yield a value of $y^+ < 1$. During grid generation, the surface elements are extruded into a volume grid which is a mixture of triangular prisms, tetrahedrals, and pyramids. The CFD++ unstructured grids ranged in size from 50 million cells for the cruise configuration to 110 million cells for the landing configuration. Force and moment coefficients were calculated by averaging the results of the last 500 iterations for each solution.

STAR-CCM+ was used at NASA ARC and is developed and distributed by CD-adapco[4]. For these simulations, the air was modeled as an ideal gas using the Reynolds-averaged Navier-Stokes, K-Omega SST (Menter) turbulence, and "All y^+" wall treatment models. Version 9.04.009 of the code was used with polyhedral meshes. Many different meshing approaches and mesh sizes were investigated to identify the effect of the mesh on the simulations. The first prism layer in the final meshes was sized to have a wall y^+ value of 1 or less.

OVERFLOW was also used by NASA ARC. The OVERFLOW code is developed and distributed by NASA LaRC[5]. Simulations were performed using OVERFLOW[6] version 2.2 on a system of overset structured grids, with grid connectivity generated by Pegasus version 5.2[7]. Spatial discretization of the Euler terms was done with the third-order HLLC upwind scheme. The time integration scheme employed depended on the nature of the solution. Runs were started with the "steady-state mode" of integration, with simple time stepping. Flows that converged to a steady state solution using this input were considered complete. At higher angles-of-attack, many flows exhibited asymptotic unsteadiness, and these solutions were solved using the "time-accurate mode," with inner iterations inside the outer second-order backward-difference time integration algorithm. Viscous fluxes were computed with second-order central spatial discretization. Solutions were computed with both the Spalart-Allmaras (SA) and SST turbulence models, which were solved with the same discretization accuracy as the mean flow variables.

USM3D was developed at NASA LaRC. It is part of the NASA Tetrahedral Unstructured Software System[8] (TetrUSS), and was used by NASA LaRC for this computational analysis. TetrUSS includes the GridTool model preparation software, the VGRID/POSTGRID volume mesh generation software and the USM3D computational flow solver[9]. The USM3D code uses the tetrahedral cell-centered, finite volume RANS method. The implicit Gauss-Seidel scheme and the Roe flux difference-splitting scheme and the SA turbulence model were used for all of the flow simulations. The code was run in first-order spatial accuracy until the residual dropped two orders of magnitude and then automatically switched to generate second-order spatially accurate solutions until full convergence. The meshes were made with a boundary layer grid normal to the wall to yield a value of $y^+ = 0.5$.

III. CFD and Wind Tunnel Results

CFD predictions were made for the HWB cruise and landing configurations in free air and in the LaRC 14'x22' and ARC 40'x80' wind tunnels. All of the results presented in this paper are for Mach number 0.20. The CFD and wind tunnel data for the cruise configuration are presented first, followed by the landing baseline Krueger configuration in free air and in the 14'x22' wind tunnel. Finally, a landing acoustic Krueger configuration is presented in free air and in the 40'x80' wind tunnel. All of these configurations are described in more detail below.

A. Cruise Configuration

Extensive CFD predictions were made before the first test in the LaRC 14'x22' wind tunnel. Figure 3 shows the HWB cruise configuration test model in the LaRC 14'x22' wind tunnel. The CFD simulations for the 14'x22' wind tunnel tests were made for the HWB in the cruise and landing configurations. Figure 4 through Figure 6 show a comparison of CFD predictions with wind tunnel results for C_L, C_D, and C_M for the cruise configuration and the vehicle in free air. The wind tunnel data in the figures are the fully-corrected data which has been processed to account for the wind tunnel walls using classical wind tunnel wall corrections. These corrections are designed to remove the effects of the wind tunnel walls but do not account for the influence of the sting on the model. For this reason, the CFD results are shown for the configurations with the model and sting in free air. Preliminary data from three wind tunnel runs are plotted to show the range of variation in the experimental data. The final wind tunnel data is pending balance calibration results and is not currently available. The r84 notation for the 14'x22' data stands for run 84. The lower

Figure 3. HWB model cruise configuration in NASA LaRC 14'x22' wind tunnel.

case “r” in the 40’x80’ key label stands for a run in the January to February 2015 wind tunnel test and the capital “R” stands for a run in the June to August 2015 wind tunnel test. This run notation is used in all of the plots. The predicted results show good agreement with the measured values of lift, drag, and pitching moment up to the stall angle. After the onset of stall there is less agreement between the predicted and measured values.

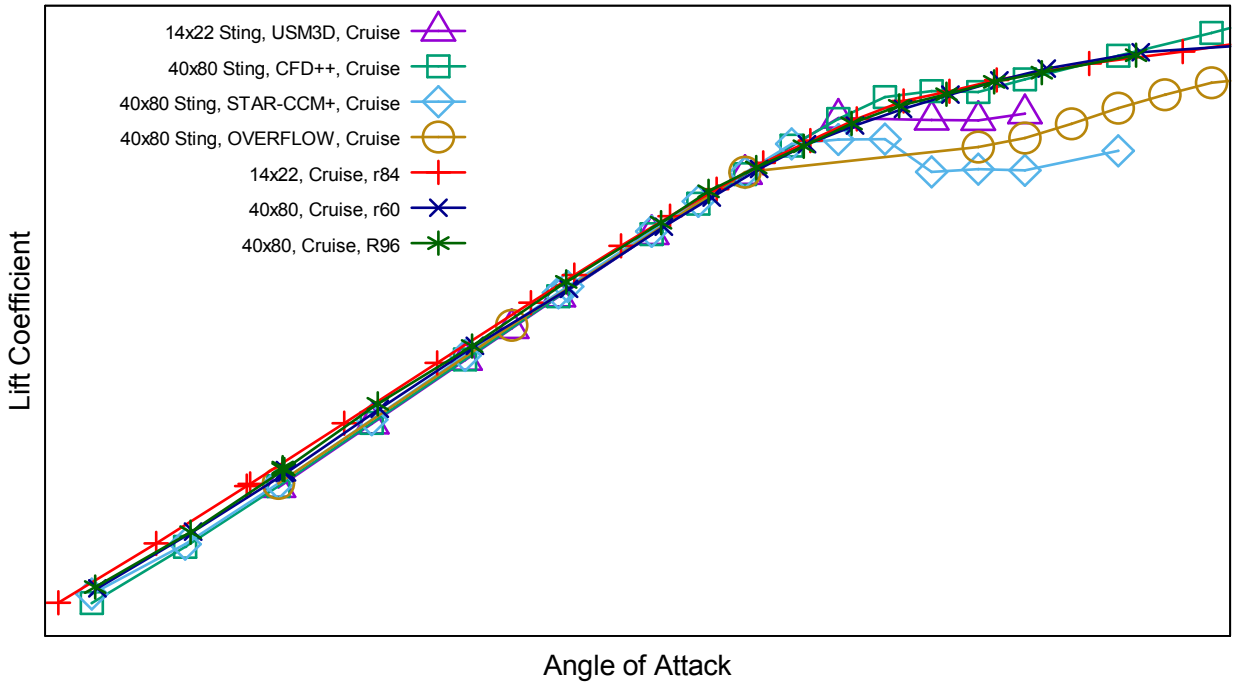

Figure 4. C_L comparisons of the cruise HWB CFD (modeled in free air) with the fully-corrected 14’x22’ and 40’x80’ wind tunnel data.

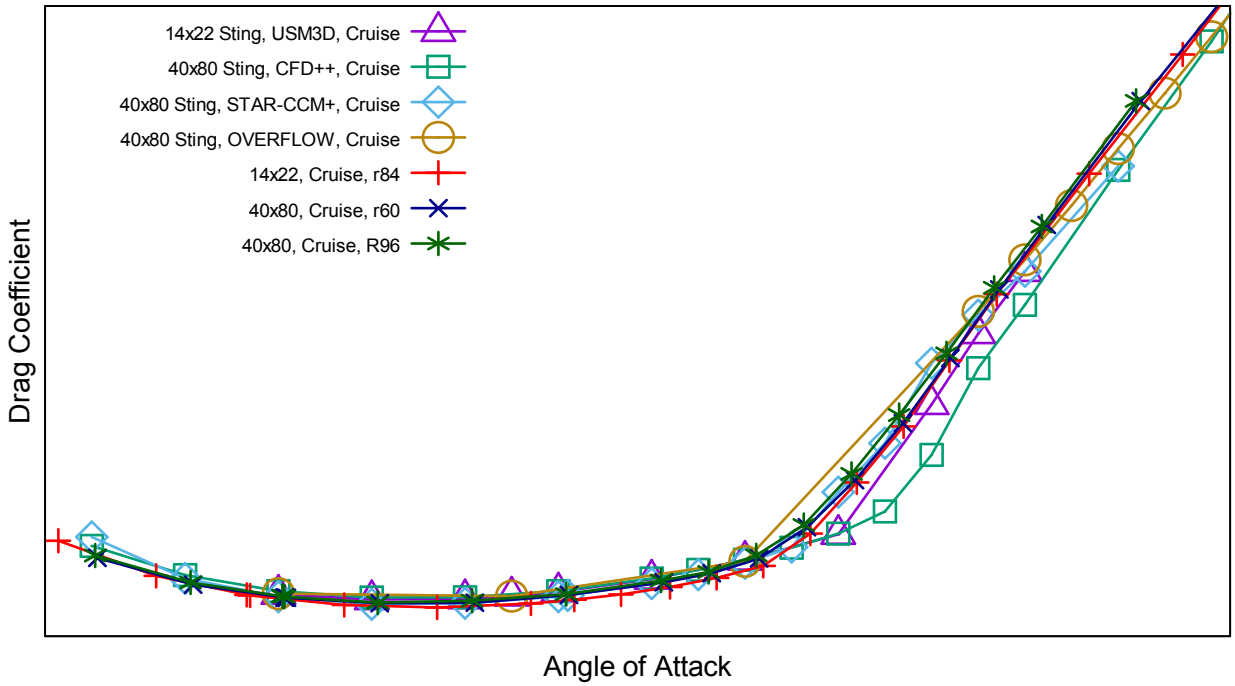

Figure 5. C_D comparisons of the cruise HWB CFD (modeled in free air) with the fully-corrected 14’x22’ and 40’x80’ wind tunnel data.

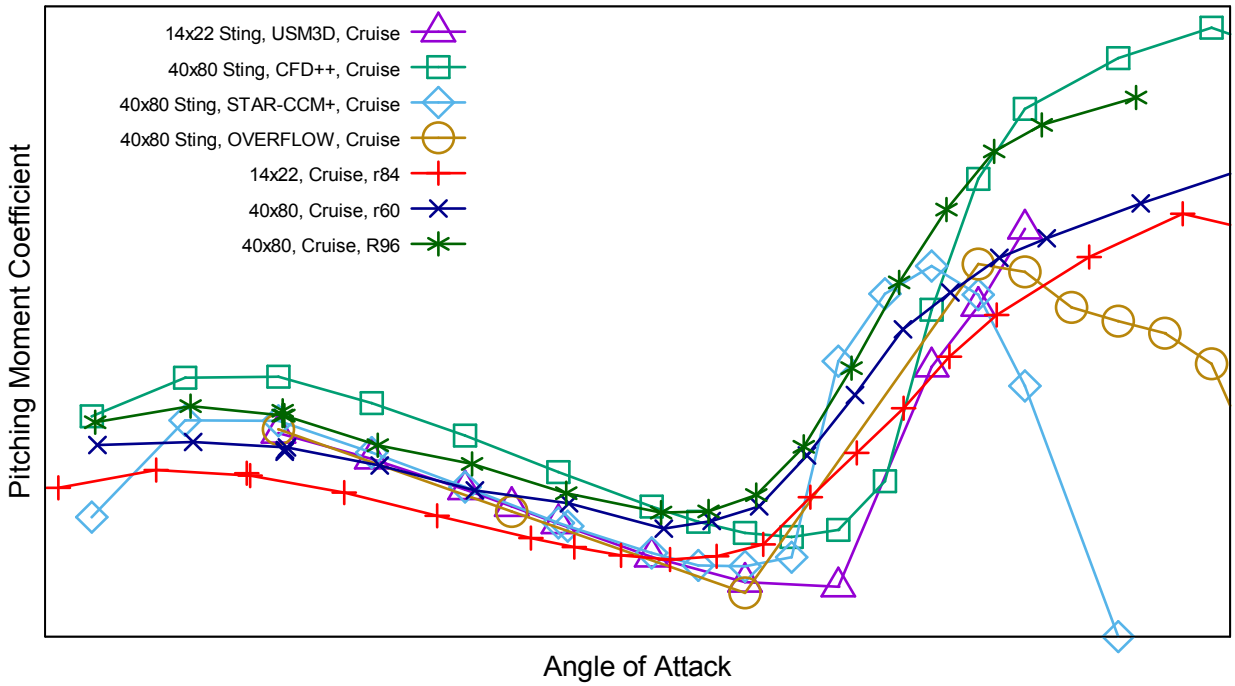

Figure 6. C_M comparisons of the cruise HWB CFD (modeled in free air) with the fully-corrected 14'x22' and 40'x80' wind tunnel data.

B. Landing 45°-2x2 Baseline Krueger Configuration in Free Air

The landing baseline Krueger flap configuration had a smooth underside as shown in Section A-A of Figure 7. After much of the CFD simulation work was completed for the 14'x22' wind tunnel test, the baseline Krueger flap was modified by creating a cutout on the underside of the flap to better represent what is expected on the full scale aircraft and its contribution to the acoustic environment. The modified flap is called the acoustic Krueger flap and is shown in Figure 7 with the baseline Krueger. The acoustic Krueger flap was tested in a matrix of positions and deployment angles in the LaRC 14'x22' wind tunnel to identify the optimal position for maximum lift. Figure 8 shows the matrix of positions for the landing and takeoff configurations and how the deployment angle was specified for the Krueger flap.

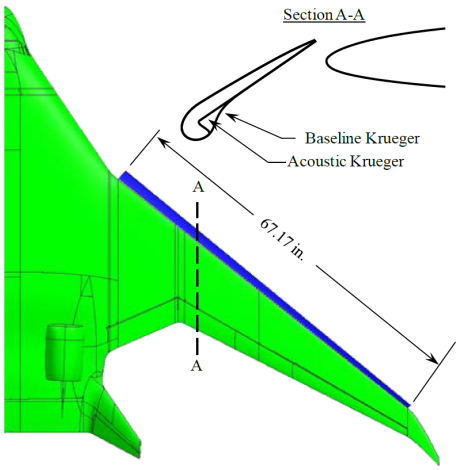

Figure 7. Baseline and Acoustic Kruegers.

The CFD simulations prior to the LaRC 14'x22' foot wind tunnel test were made with the baseline Krueger in the 45°-2x2 position Where the 45° refers to the flap deflection angle and the '2x2' refers to the 'L22' landing Krueger location depicted in the matrix shown on the upper left of Figure 8. One entry was completed in the 14'x22' wind tunnel test with the baseline Krueger in the 45°-2x2 position to provide

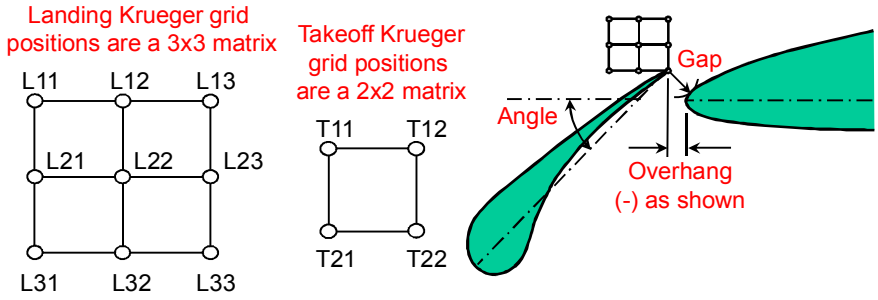

Figure 8. Illustration of Krueger grid positions and angle.

validation data for the CFD codes. Figure 9 through Figure 11 show a comparison of the CFD predictions with the preliminary 14'x22' fully-corrected wind tunnel data for C_L, C_D, and C_M. The CFD predictions included the sting.

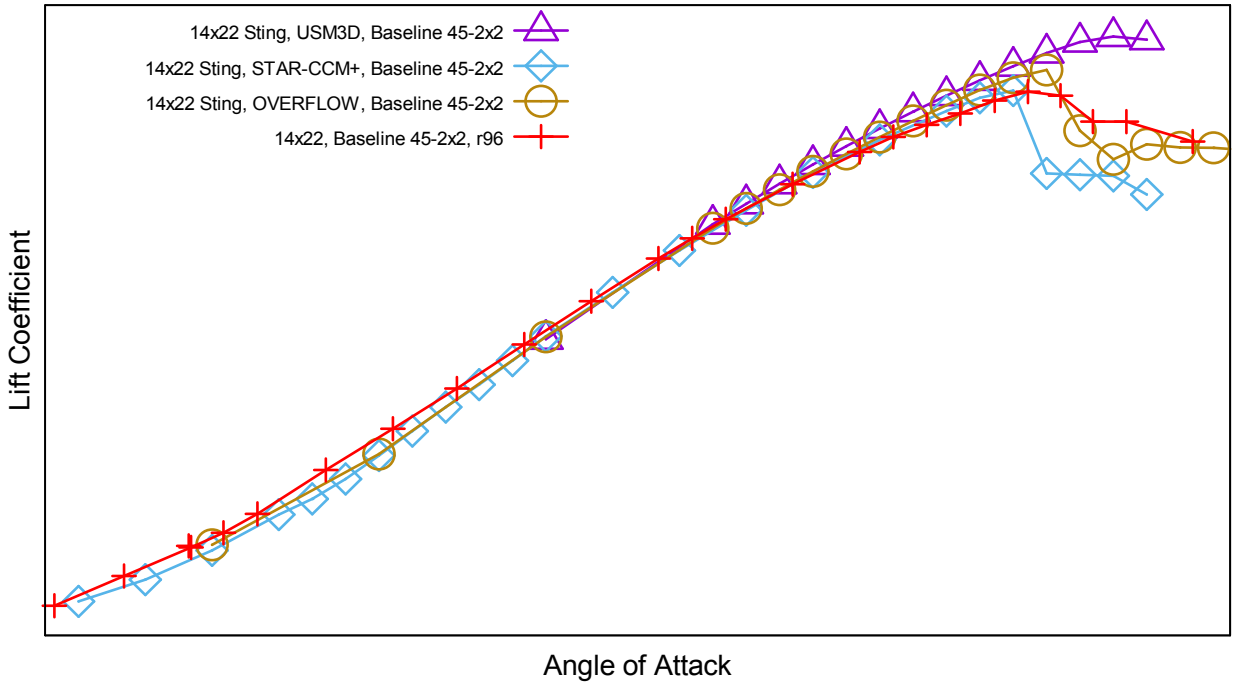

Figure 9. C_L comparisons of the baseline 45°-2x2 Krueger HWB CFD (modeled in free air) with the fully-corrected 14'x22' wind tunnel data.

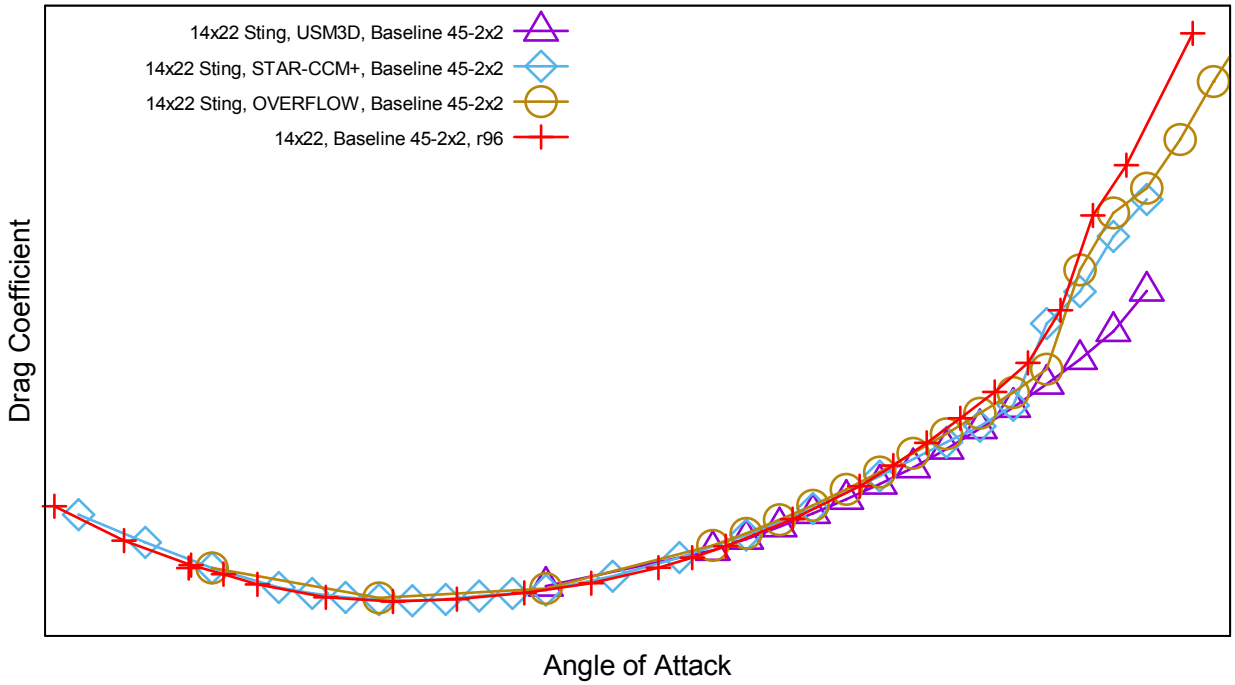

Figure 10. C_D comparisons of the baseline 45°-2x2 Krueger HWB CFD (modeled in free air) with the fully-corrected 14'x22' wind tunnel data.

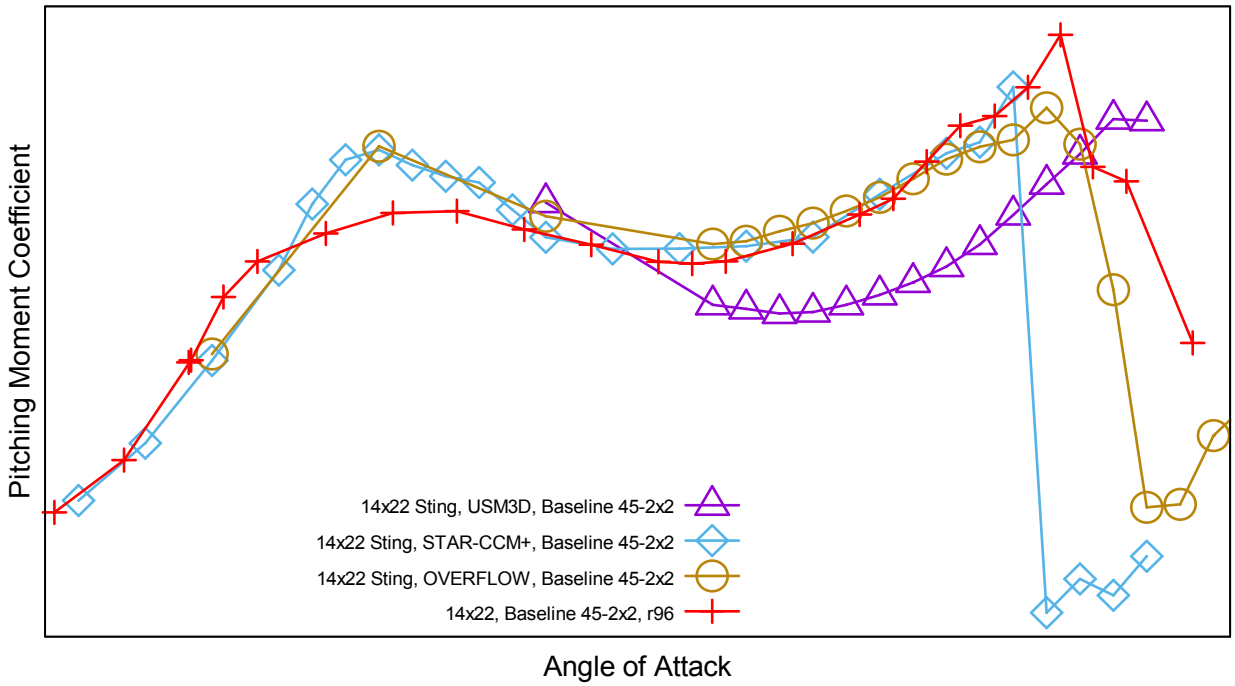

Figure 11. C_M comparisons of the baseline 45°-2x2 Krueger HWB CFD (modeled in free air) with the fully-corrected 14'x22' wind tunnel data.

C. Landing Baseline 45°-2x2 Krueger Configuration in the 14'x22' Wind Tunnel

CFD simulations were computed using two of the codes for the baseline 45° -2x2 Kueger configuration in the 14'x22' wind tunnel. To make the wind tunnel more manageable to simulate, it was modeled with a constant cross section and a slip boundary condition on the wind tunnel walls. The 161" x 174" (13.4'x22') cross section shown in Figure 12 was used in the CFD simulations. The shorter height takes into account the boundary layer thickness at the model location in the wind tunnel.

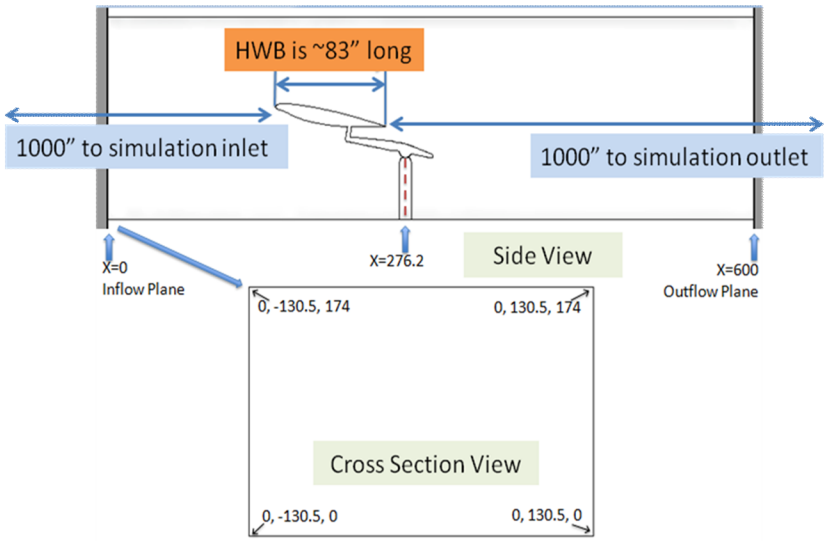

Figure 12. 14'x22' Wind tunnel CFD model.

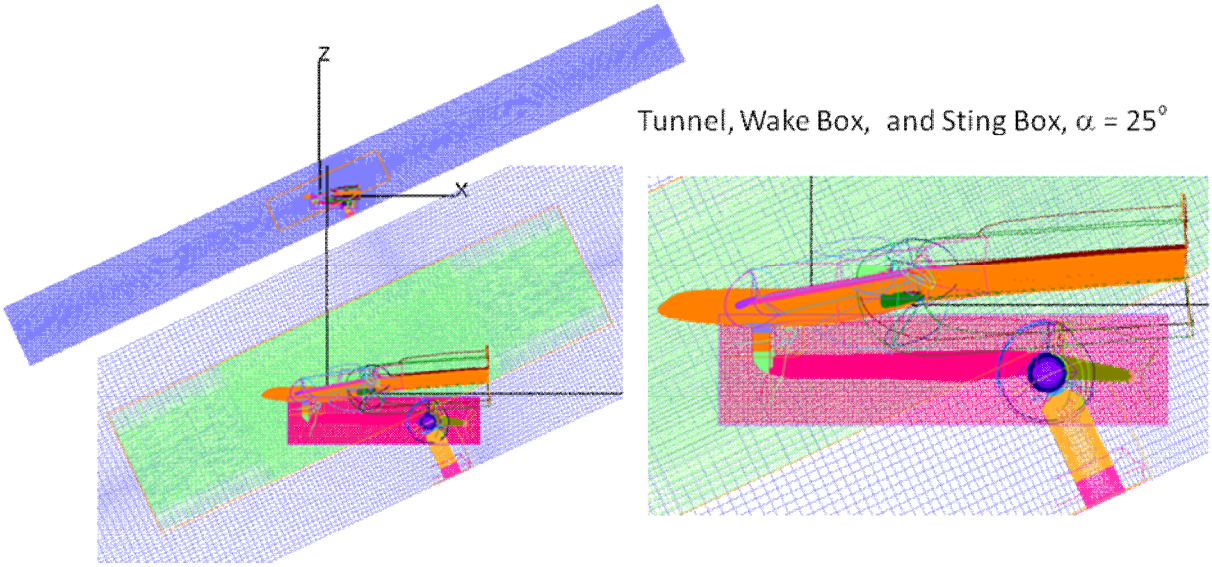

Figure 13. OVERFLOW meshing approach for 14'x22' wind tunnel simulations.

The OVERFLOW simulations modeled the tunnel test section as being twice as long as the 600 inch long test section shown in Figure 12, and the STAR-CCM+ simulations similarly modeled it as extending 1000" fore and aft of the model. The tunnel length was extended in these CFD simulations so as to isolate the HWB model flow from the CFD domain inlet and outlet boundaries. Figure 13 shows the overset meshing strategy used in the OVERFLOW simulations for $\alpha = 25°$. Figure 14 - Figure 16 show the C_L, C_D, and C_M values for the baseline configuration for the CFD codes and the 14'x22' wind tunnel test data. In this case, the wind tunnel uncorrected values are the most appropriate to use when comparing these CFD data to the wind tunnel measurements. The fully-corrected wind tunnel measurements are included to show their variation from the uncorrected values. These figures show that the addition of modeling the wind tunnel walls in the CFD simulations improves the CFD agreement with the experimental data for some angles of attack.

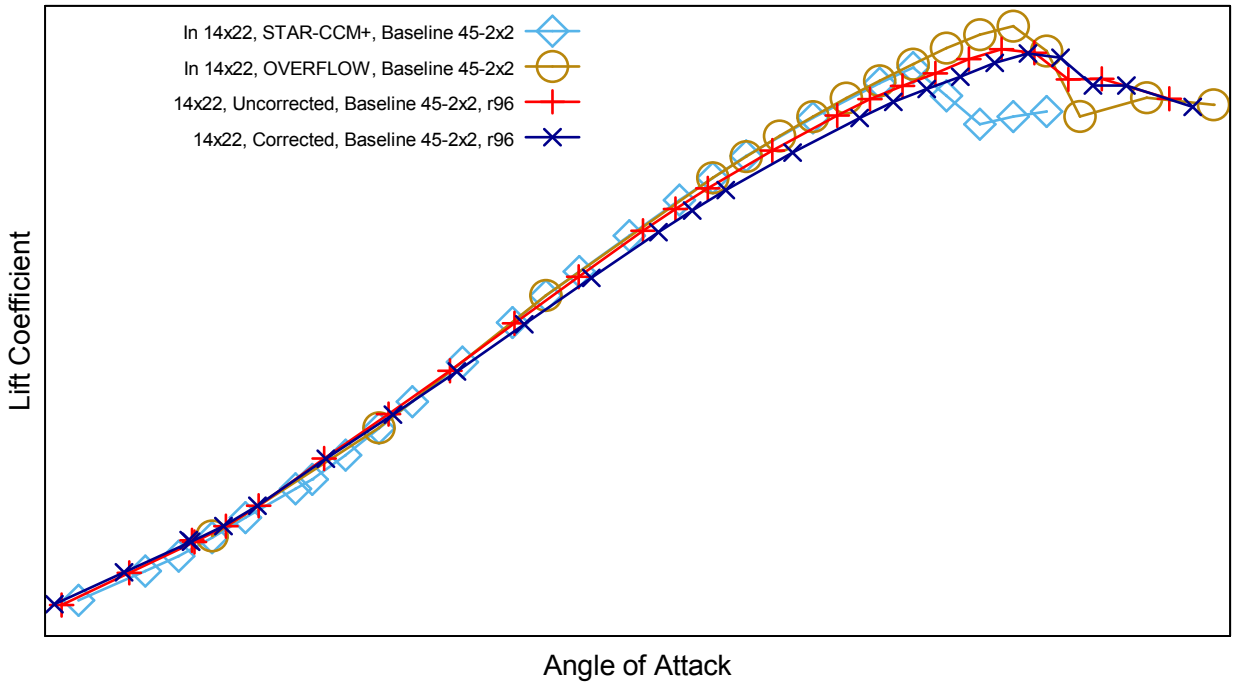

Figure 14. C_L comparisons of the baseline 45°-2x2 Krueger HWB CFD (modeled in the 14'x22' wind tunnel) with the uncorrected and fully-corrected 14'x22' wind tunnel data.

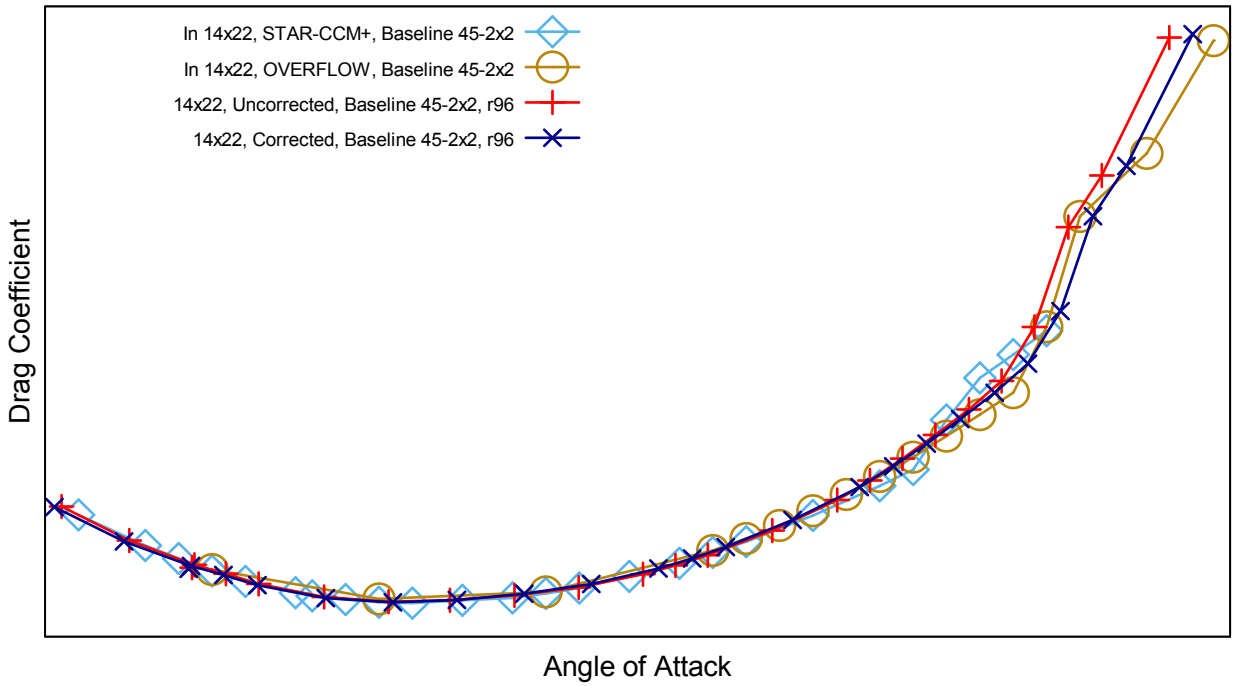

Figure 15. C_D comparisons of the baseline 45°-2x2 Krueger HWB CFD (modeled in the 14'x22' wind tunnel) with the uncorrected and fully-corrected 14'x22' wind tunnel data.

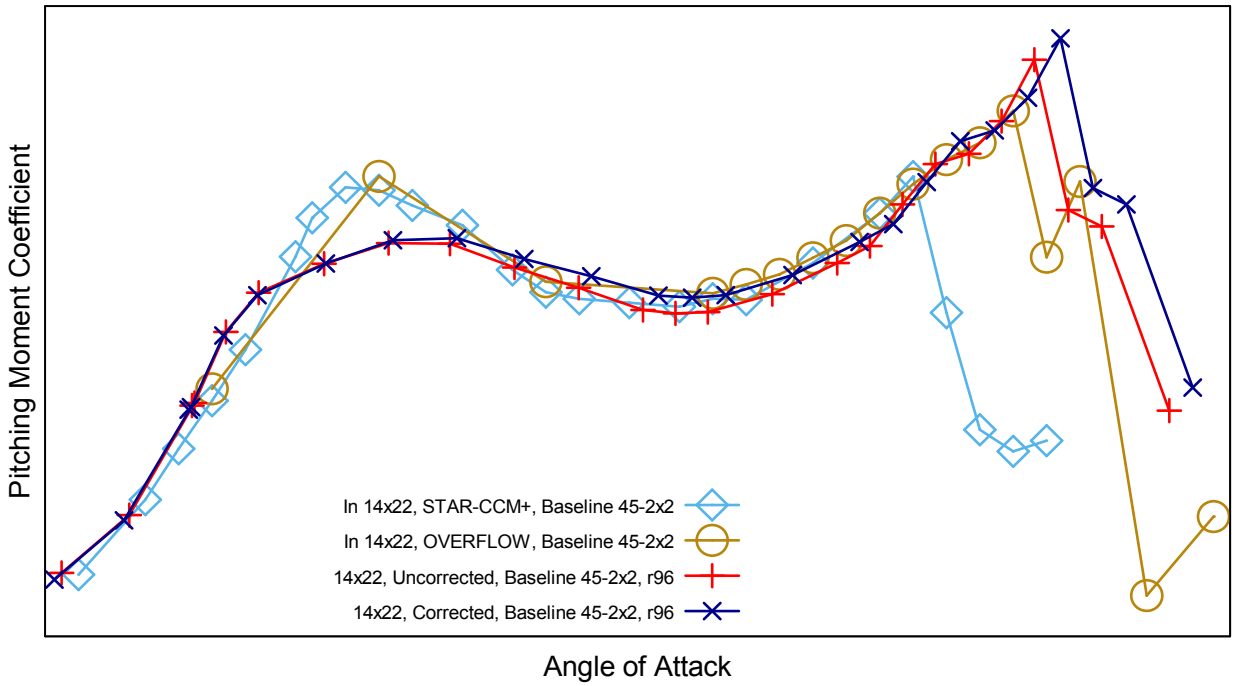

Figure 16. C_M comparisons of the baseline 45°-2x2 Krueger HWB CFD (modeled in the 14'x22' wind tunnel) with the uncorrected and fully-corrected 14'x22' wind tunnel data.

D. Landing Acoustic 45°-3x2 Krueger Configuration in Free Air

After the LaRC 14'x22' wind tunnel testing was complete, the model was tested in the NASA ARC 40'x80' wind tunnel. Figure 17 shows the model installed in the NASA ARC 40'x80' wind tunnel. Large and small acoustic arrays were installed near the tunnel floor to the left of the model. For these tests, the baseline configuration was the acoustic flap in the landing 45^{o}-3x2 position (Figure 8). Three of the CFD codes were used to make simulations for this new configuration. While the 14'x22' wind tunnel CFD simulations were run without the Krueger flap structural brackets, the 40'x80' wind tunnel simulations were run with five structural brackets on each wing. Figure 18 shows a top view of the structural brackets and the 40'x80' wind tunnel sting and vertical support. A bottom view of brackets with a close up of the surface mesh on the center bracket is shown in Figure 19. Figure 20 – Figure 22 show the C_L, C_D, and C_M values for the acoustic configuration for the CFD codes and the 14'x22' and 40'x80' wind tunnel tests. The predicted results again show good agreement with the measured values of lift, and drag up to the stall angle. The pitching moment plot shows slightly larger variation in the different predicted CFD results but for the most part the CFD results follow the same trend as the measured results up to the stall angle. After the onset of stall there is less agreement between the predicted and measured values.

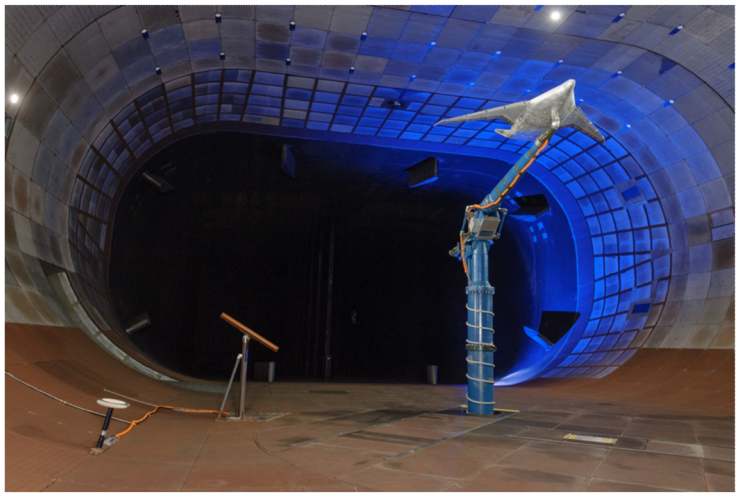

Figure 17. HWB model in the ARC 40'x80' wind tunnel.

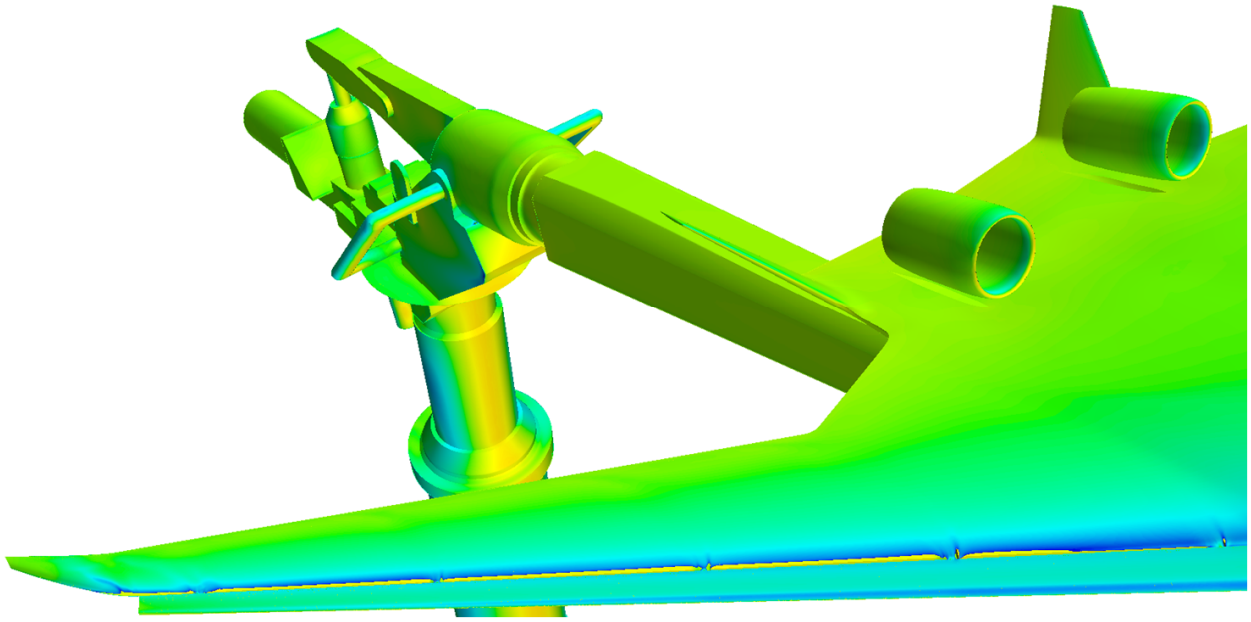

Figure 18. Top view of the right wing pressure distribution showing flap brackets and 40'x80' sting and support.

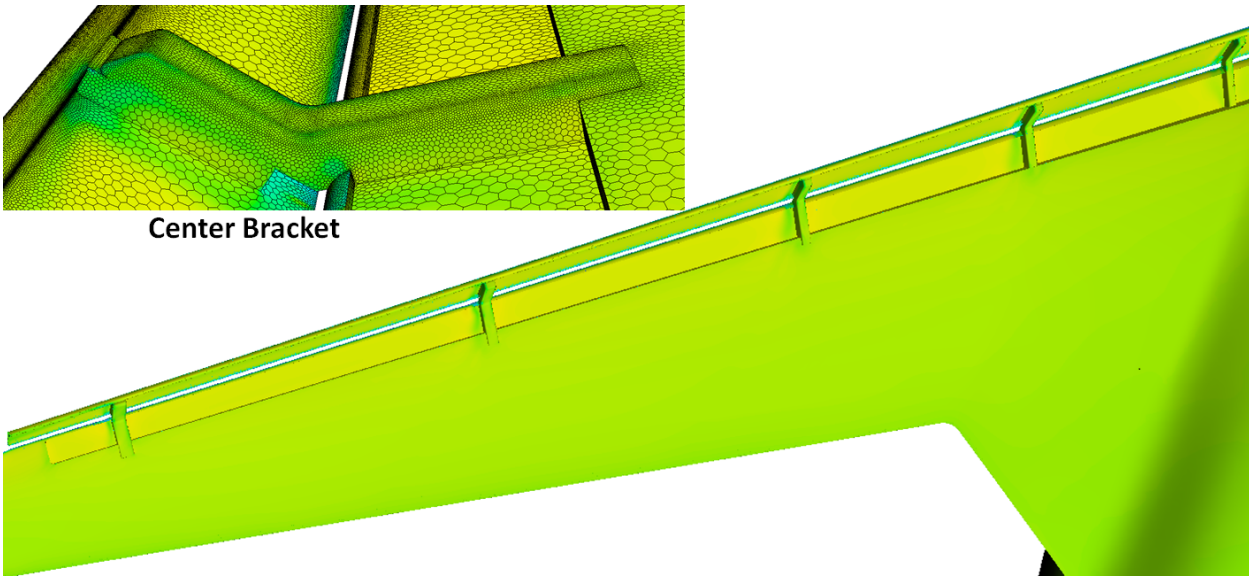

Figure 19. Bottom view of right wing pressure distribution showing flap brackets, acoustic Krueger flap shape, and flap well.

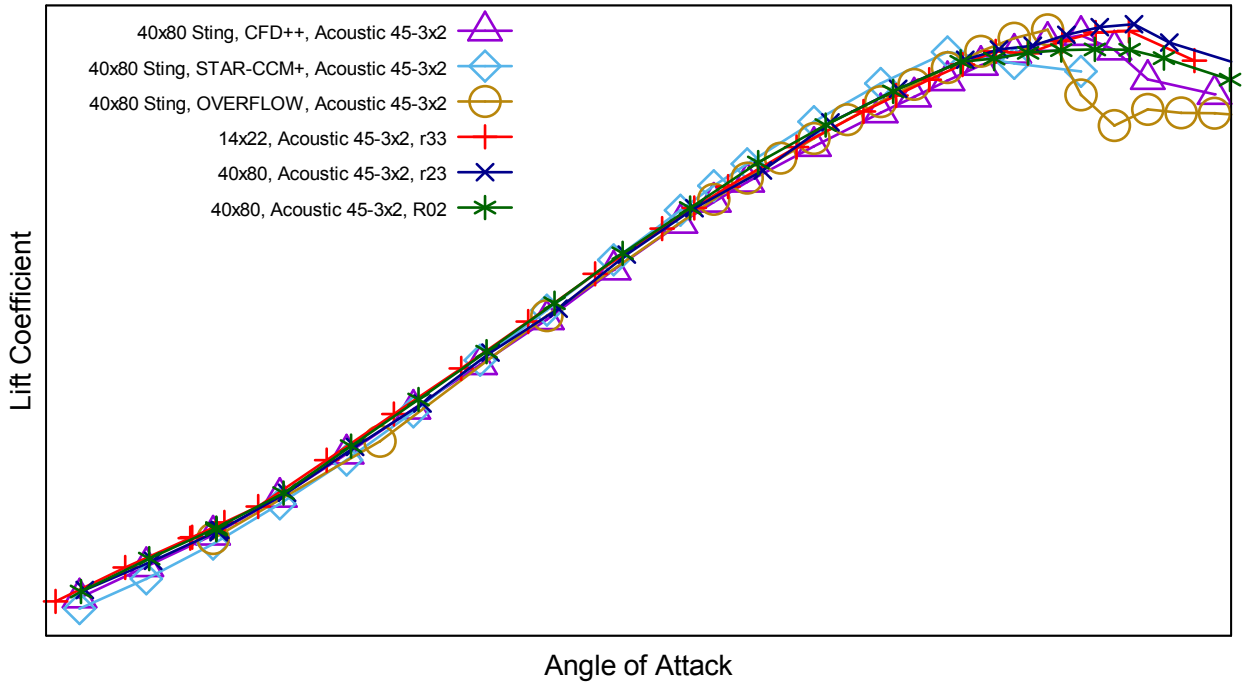

Figure 20. C_L comparisons of the acoustic 45°-3x2 Krueger HWB CFD (modeled in free air) with the fully-corrected 14'x22' and 40'x80' wind tunnels data.

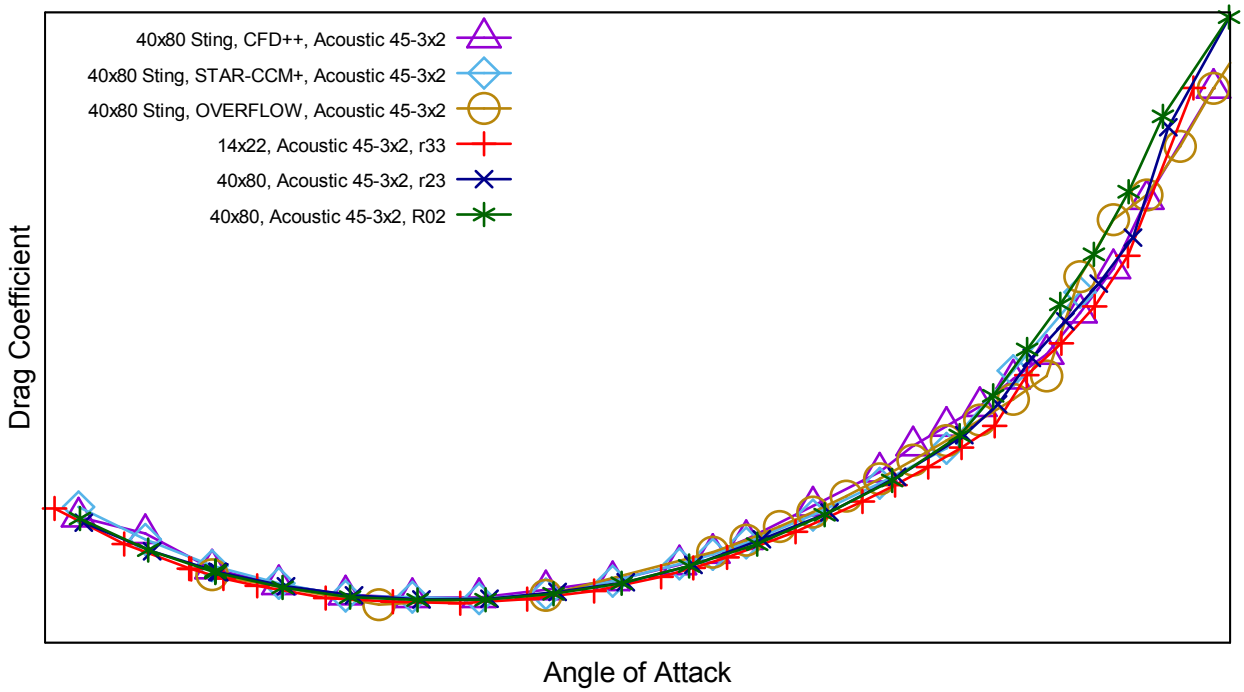

Figure 21. C_D comparisons of the acoustic 45°-3x2 Krueger HWB CFD (modeled in free air) with the fully-corrected 14'x22' and 40'x80' wind tunnels data.

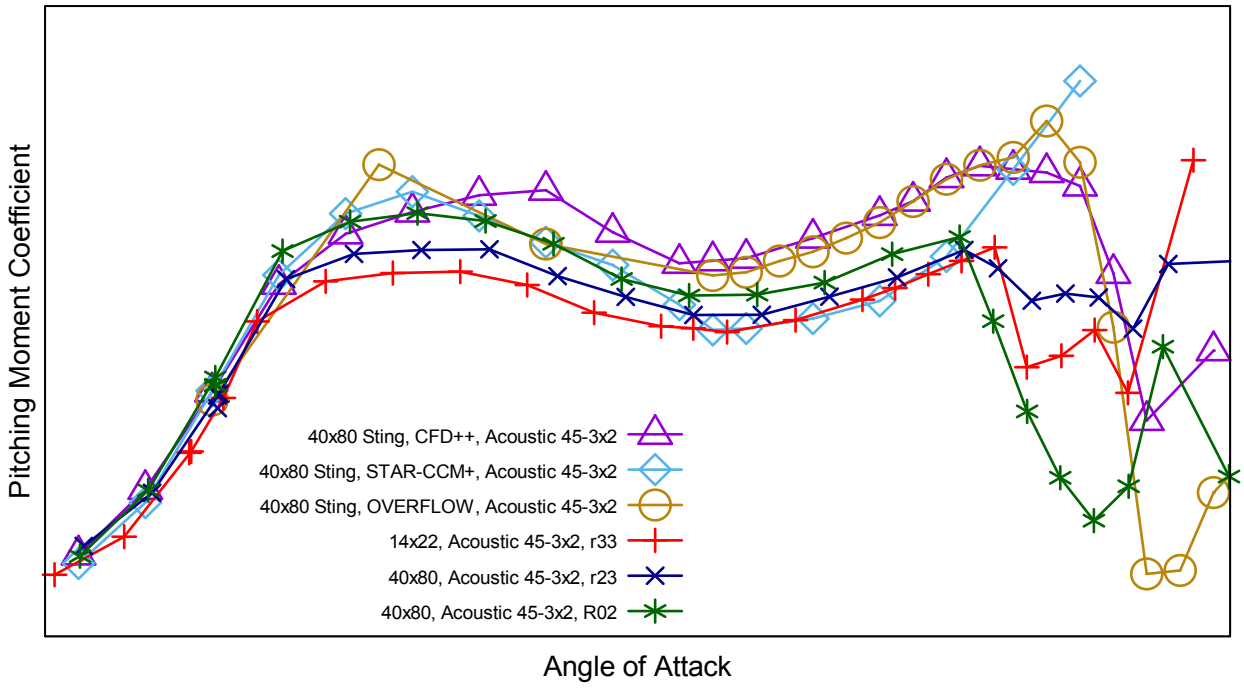

Figure 22. C_M comparisons of the acoustic 45°-3x2 Krueger HWB CFD (modeled in free air) with the fully-corrected 14'x22' and 40'x80' wind tunnels data.

E. Landing Acoustic 45°-3x2 Krueger Configuration in the 40'x80' Wind Tunnel

To investigate the effect of the wind tunnel walls on the measured forces and moments, the HWB was modeled in the ARC 40'x80' wind tunnel with the sting and support post included using the OVERFLOW and STAR-CCM+

codes. For the OVERFLOW simulations, the wind tunnel was modeled with a constant cross section with the size and shape of the 40'x80' wind tunnel test section. Again, a slip wall boundary condition was used for the OVERFLOW wind tunnel walls. This is the same process that was used for modeling the 14'x22' wind tunnel.

For the STAR-CCM+ code, the wind tunnel was modeled from the beginning of the inlet diffuser to the end of the outlet diffuser as shown in Figure 23. The 40'x80' wind tunnel has large vortex generators on the tunnel walls at the beginning of the outlet diffuser. These vortex generators were also included in the STAR-CCM+ simulations as shown in Figure 24. Due to the presence of the 40'x80' wind tunnel in the computational domain, a mesh had to be created for each angle-of-attack modeled. These meshes ranged in size from 120 million to 129 million polyhedral cells. The wind tunnel walls were modeled with a viscous boundary condition.

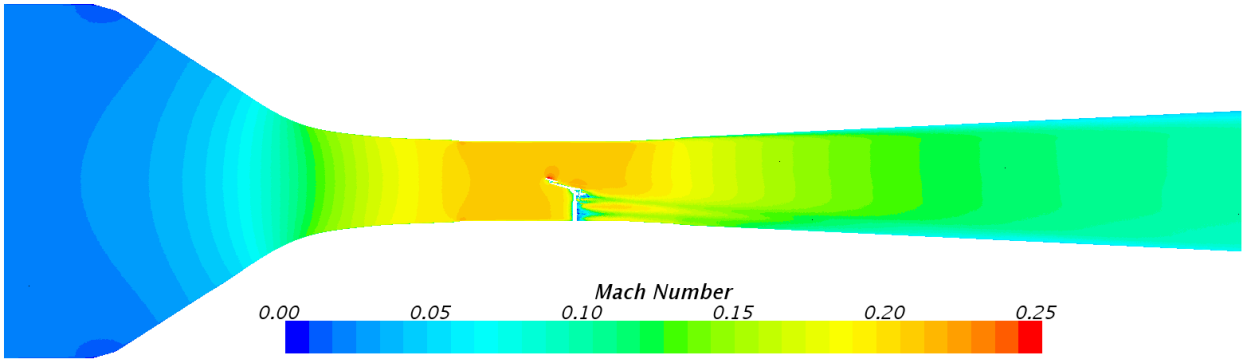

Figure 23. STAR-CCM+ Mach number on symmetry plane for 40'x80' wind tunnel simulation for α = 15°.

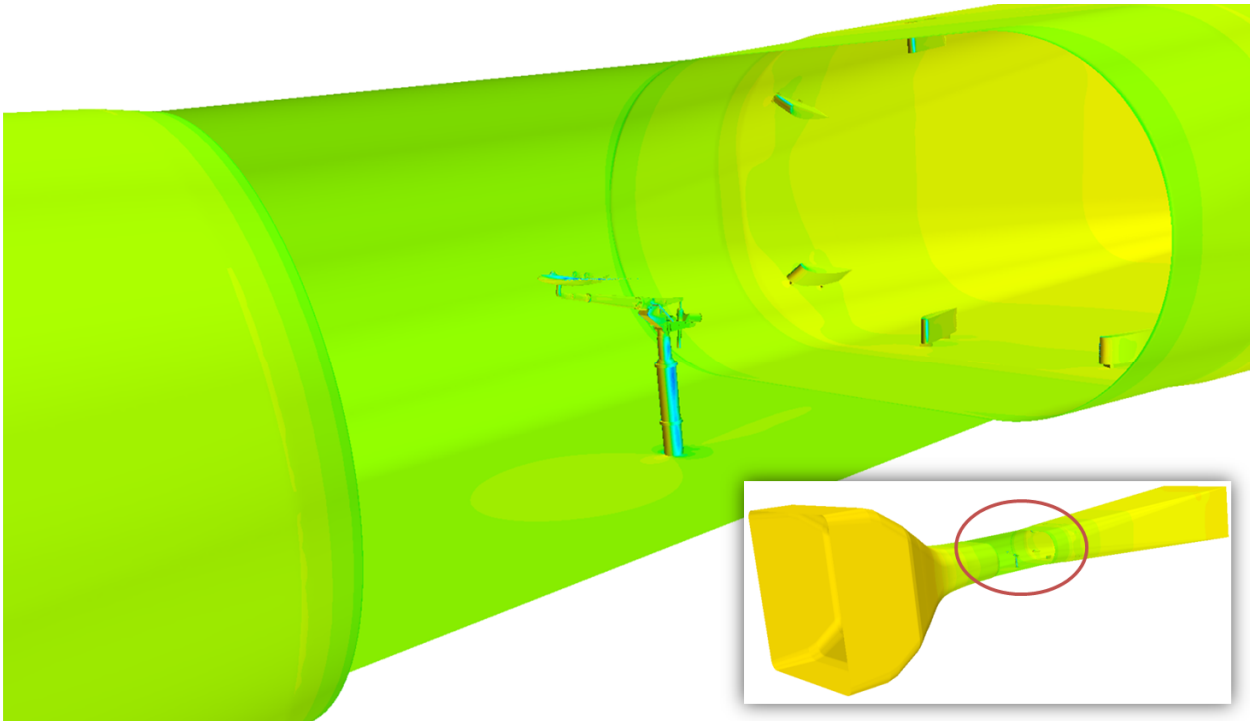

Figure 24. STAR-CCM+ Pressure Coefficient of 40'x80' wind tunnel simulation for α = 15°.

Figure 25 - Figure 27 show the CFD predictions and the preliminary wind tunnel results for C_L, C_D, and C_M for the acoustic Krueger flap with structural brackets in the ARC 40'x80' wind tunnel. The wind tunnel data included in the plots are the uncorrected values that have not been processed to account for the wind tunnel walls or the sting. These figures show an improved agreement between the CFD predictions and the wind tunnel data when the wind tunnel walls are included in the simulations.

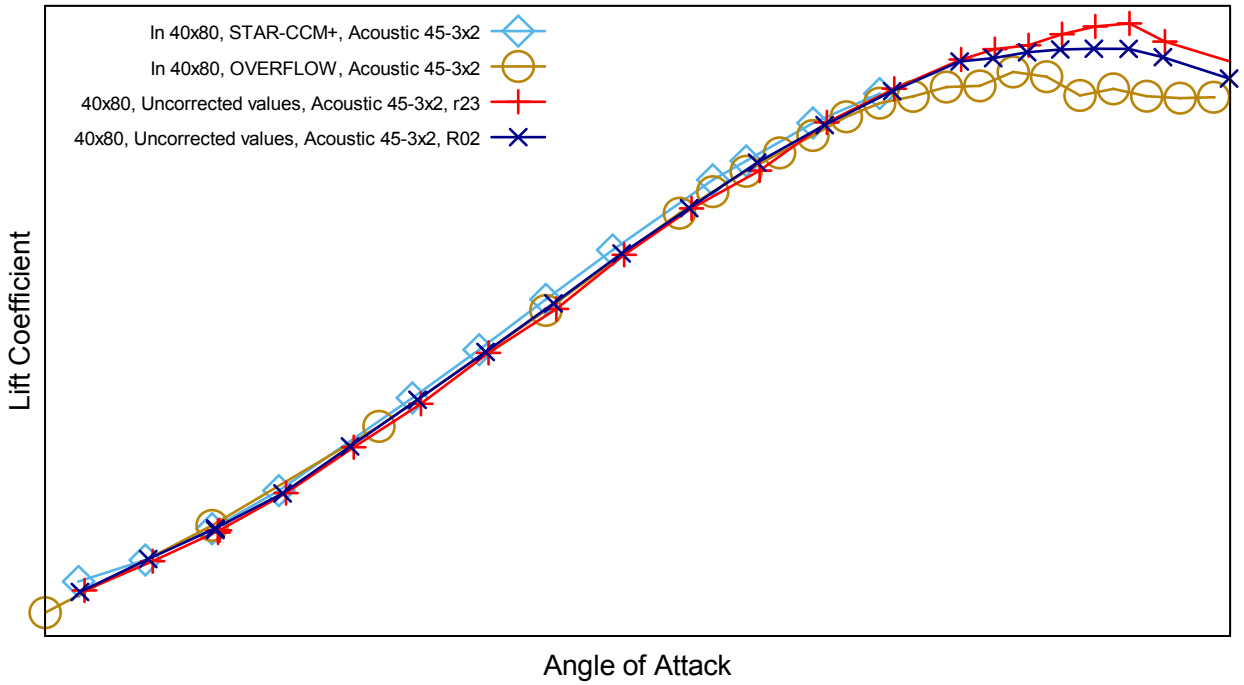

Figure 25. C_L comparisons of the acoustic 45°-3x2 Krueger HWB CFD (modeled in the 40'x80' wind tunnel) with the uncorrected 40'x80' wind tunnel data.

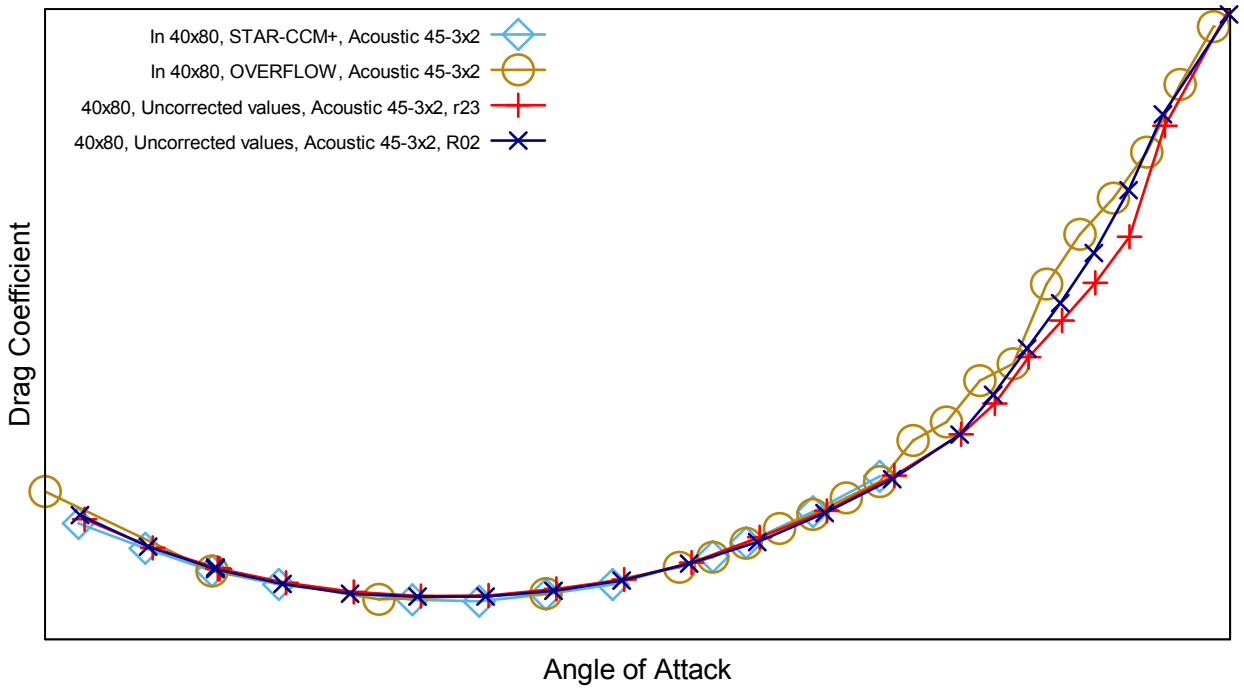

Figure 26. C_D comparisons of the acoustic 45°-3x2 Krueger HWB CFD (modeled in the 40'x80' wind tunnel) with the uncorrected 40'x80' wind tunnel data.

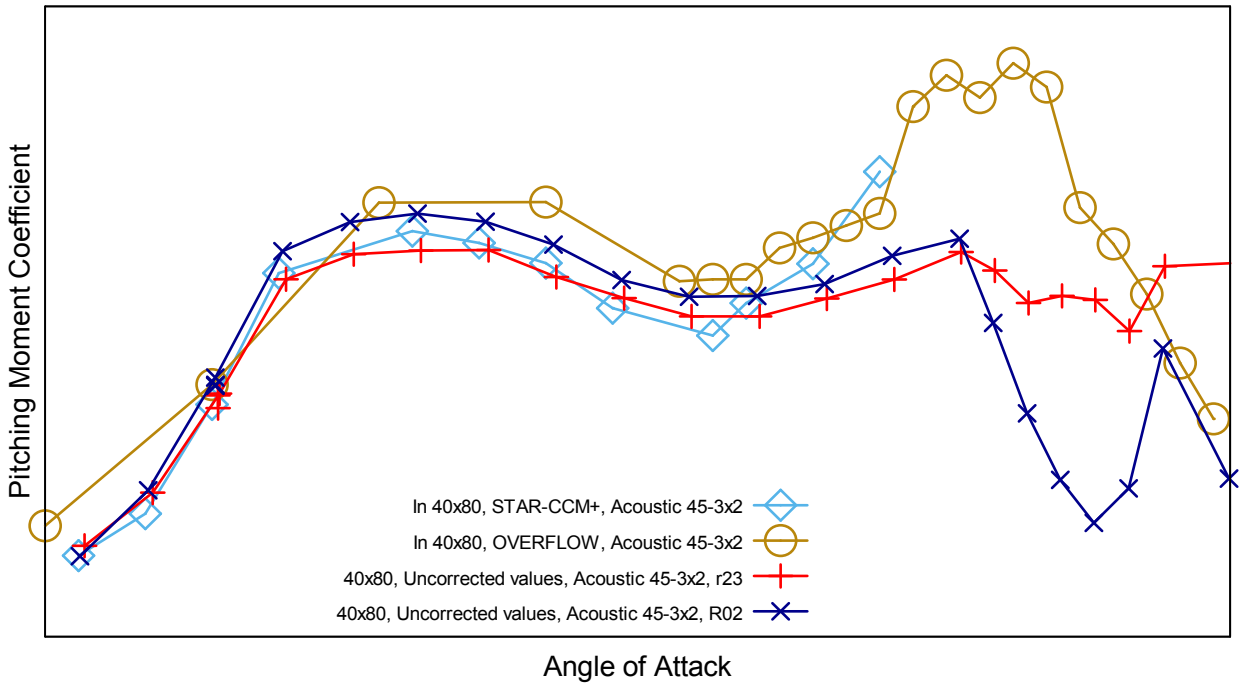

Figure 27. C_M comparisons of the acoustic 45°-3x2 Krueger HWB CFD (modeled in the 40'x80' wind tunnel) with the uncorrected 40'x80' wind tunnel data.

F. Summary of CFD Predictions

Table 1 shows a matrix of the CFD predictions and wind tunnel data included in this report. None of the configurations were run by all of the codes. For the CFD simulations of the HWB in a wind tunnel with the sting and support, the tunnel modeled is listed in the table.

	14'x22'	40'x80'	USM3D	CFD++	STAR-CCM+	OVERFLOW
Cruise with 14'x22' Sting in Free Air			x			
Cruise with 40'x80' Sting in Free Air				x	x	x
Cruise in Tunnel	x	x				
Baseline Krueger 45°-2x2 with 14'x22' sting in Free Air			x		x	x
Baseline Krueger 45°-2x2 in Tunnel	x				14'x22'	14'x22'
Acoustic Krueger 45-3x2 with 40'x80' sting.				x	x	x
Acoustic Krueger 45-3x2 in Tunnel	x	x			40'x80'	40'x80'

Table 1. Matrix of CFD predictions and wind tunnel results.

IV. Conclusion

CFD simulations were performed before and after testing the 5.75% scale model of the Boeing 0009GM HWB in the NASA LaRC 14'x22' and NASA ARC 40'x80' wind tunnels. The results presented show the level of agreement between the results from the two wind tunnel tests and the CFD predictions from four different codes. The predicted results demonstrate good agreement with the measured results up to the stall angle of attack and less agreement after the onset of stall. The predicted results also show that including the tunnel walls in the CFD simulations increases the agreement with the experimental data.

Acknowledgments

The research reported in this paper was sponsored by the NASA Integrated Aviation Systems Research Program's Environmentally Responsible Aviation Project. Much of the computer resources used for the CFD predictions in this report were provided by NASA.

References

[1] Dickey, E. D., Princen, N. H., Bonet, J. T., and Ige, G. K., "Wind Tunnel Model Design and Fabrication of a 5.75% Scale Blended-Wing-Body Twin Jet Configuration," *AIAA SciTec 2016*, Washington, DC, Jan. 2016.
[2] Metacomp Technologies website, http://MetaCompTech.com [retrieved 30 Oct 2015].
3 Pointwise Software website, http://Pointwise.com [retrieved 30 Oct 2015].
4 CD-adapco website, http://CD-adapco.com [retrieved 30 October 2015].
5 Buning, P. G., NASA OVERFLOW CFD Code website, http://OVERFLOW.LaRC.nasa.gov, [retrieved 30 Oct 2015].
6 Tramel, R. W., Nichols R. H., and Buning P. G., "Addition of Improved Shock-Capturing Schemes to OVERFLOW 2.1," AIAA-2009-3988.
7 Suhs, N. E. Rogers, S. E., and Dietz, W. E. "PEGASUS 5: An Automated Pre-processor for Overset-Grid CFD," AIAA Paper 2002-3186, AIAA Fluid Dynamics Conference, June 2002, St. Louis, MO.
8 Frink, N. T., Tetrahedral Unstructured Software System (TetrUSS) website, http://TetrUSS.LaRC.NASA.Gov [retrieved 30 October 2015].
9 Pandya, M. J., Abdol-Hamid, K. S., and Frink, N. T., "Enhancement of USM3D Unstructured Flow Solver for High-Speed High-Temperature Shear Flows," AIAA 2009-1329, The 47th AIAA Aerospace Sciences Meeting, January 5-8, 2009.

NASA Environmentally Responsible Aviation Hybrid Wing Body Flow-Through Nacelle Wind Tunnel CFD

Michael J. Schuh[1] and Joseph A. Garcia[2]
NASA Ames Research Center, Moffett Field, CA, 94035, USA

Melissa B. Carter[3] and Karen A. Deere[3]
NASA Langley Research Center, Hampton VA, 23681, USA

Paul M. Stremel[4]
Science and Technology Corporation, NASA Research Park, CA, 94035, USA

and

Daniel M. Tompkins[5]
Boeing Research & Technology, Huntington Beach, CA, 92647, USA

Wind tunnel tests of a 5.75% scale model of the Boeing Hybrid Wing Body (HWB) configuration were conducted in the NASA Langley Research Center (LaRC) 14'x22' and NASA Ames Research Center (ARC) 40'x80' low speed wind tunnels as part of the NASA Environmentally Responsible Aviation (ERA) Project. Computational fluid dynamics (CFD) simulations of the flow-through nacelle (FTN) configuration of this model were performed before and after the testing. This paper presents a summary of the experimental and CFD results for the model in the cruise and landing configurations.

Nomenclature

α	=	Angle of Attack
C_D	=	drag coefficient
C_L	=	lift coefficient
C_M	=	moment coefficient
y^+	=	nondimensional first cell height

Acronyms

ARC	=	Ames Research Center
CFD	=	computational fluid dynamics
ERA	=	Environmentally Responsible Aviation
FTN	=	flow-through nacelle
HWB	=	hybrid wing body
LaRC	=	Langley Research Center
NAS	=	NASA Advanced Supercomputing
NASA	=	National Aeronautics and Space Administration
RANS	=	Reynolds-averaged Navier-Stokes
SA	=	Spalart-Allmaras
SST	=	shear stress transport

[1] Aerospace Engineer, System Analysis Office, Aeronautics Directorate, Mail Stop 258-1.
[2] Aerospace Engineer, System Analysis Office, Aeronautics Directorate, Mail Stop 258-1, AIAA Senior Member.
[3] Aerospace Engineer, Configuration Aerodynamics Branch, Mail Stop 499, AIAA Senior Member.
[4] Senior Research Scientist, Mail Stop 258-1, AIAA Member.
[5] Propulsion Engineer, Flight & Vehicle Technology, Boeing Research & Technology, AIAA Senior Member.

I. Introduction

NASA's Environmentally Responsible Aviation (ERA) Project explores enabling technologies to reduce aviation's impact on the environment. One research challenge area for the project has been studying advanced airframe and engine integration concepts to reduce community noise and fuel burn. In order to achieve this, wind tunnel tests at both the NASA LaRC 14'x22' and the NASA ARC 40'x80' low speed wind tunnels have been conducted on a 5.75% scale model of the Boeing Hybrid Wing Body (HWB) 0009GM[1] configuration. These wind tunnel tests entailed various entries to evaluate the propulsion airframe interference including aerodynamic performance and aeroacoustics. In order to baseline the powered configurations being tested, a simplified engine modeled as a flow-through nacelle (FTN) configuration was tested as well. This paper provides a summary of CFD simulations from four different flow solvers that were conducted in advance of the FTN test in support of model integration hardware design as well as some post-test aerodynamic performance data comparisons. Figure 1 shows computed pressure coefficient contours on the HWB in the 40'x80' wind tunnel.

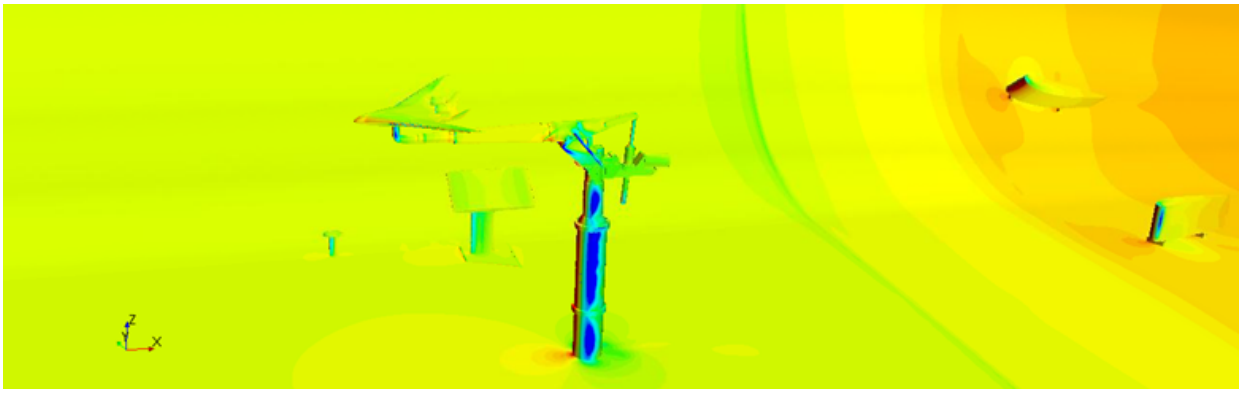

Figure 1. CFD solution within the ARC 40'x80' wind tunnel facility.

Figure 2 shows a configuration of the ERA HWB model tested in the wind tunnels. CFD simulations were performed in the months prior to testing. The HWB model was tested in the 14'x22' wind tunnel during July of 2014. It was tested in the 40'x80' wind tunnel during January and February of 2015 and again during June to August of 2015. Data were collected for the model in the FTN configuration during each of these test periods.

This paper presents simulation results for four different CFD codes, CFD++, OVERFLOW, STAR-CCM+, and USM3D and the wind tunnel test data for the FTN model in both the landing and cruise configurations. CFD predictions were made for the model in free air, free air with the wind tunnel sting, and in the wind tunnels with the sting, vertical support structures and walls.

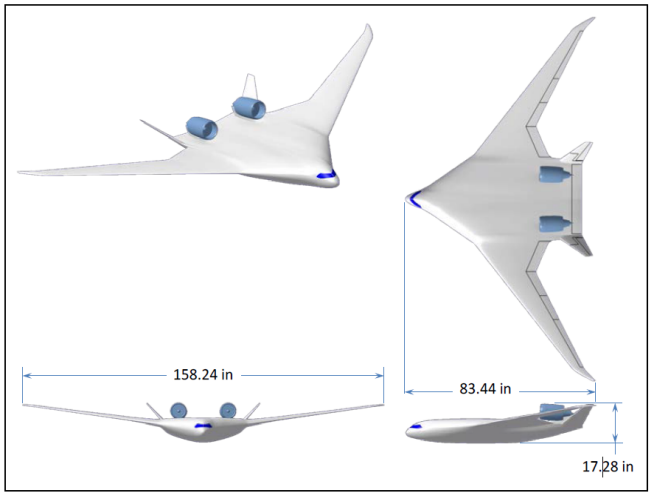

Figure 2. HWB vehicle.

II. CFD Codes

Four codes were used to simulate various configurations of the HWB vehicle. The HWB cruise and landing configurations were simulated in free air and in the two wind tunnels. The free air simulations were made without and with the wind tunnel sting. The descriptions of the four CFD codes used in this effort are presented next followed by comparisons of the CFD simulation results with the 14'x22' and 40'x80' wind tunnel measurements.

CFD++ was used by Boeing to perform Reynolds-averaged Navier-Stokes (RANS) simulations on unstructured grids. CFD++ is available from Metacomp Technologies[2]. The primary turbulence model employed was the two-equation realizable k-epsilon model. The grids were created with the Pointwise[3] software. The local grid spacing was set to yield a value of $y^+ < 1$. During grid generation, the surface elements are extruded into a volume grid which is a mixture of triangular prisms, tetrahedrals, and pyramids. The CFD++ unstructured grids ranged in size

from 50 million cells for the cruise configuration to 110 million cells for the landing configuration. Force and moment coefficients were calculated by averaging the results of the last 500 iterations for each solution.

STAR-CCM+ was used at NASA ARC and is developed and distributed by CD-adapco[4]. For these simulations, the air was modeled as an ideal gas using the Reynolds-averaged Navier-Stokes, K-Omega SST (Menter) turbulence, and "All y^+" wall treatment models. Version 9.04.009 of the code was used with polyhedral volume meshes. Many different meshing approaches and mesh sizes were investigated to identify the effect of the mesh on the simulations. The first prism layer in the final meshes was sized to have a wall y^+ value of 1 or less.

OVERFLOW was also used by NASA ARC. The OVERFLOW code is developed and distributed by NASA LaRC[5]. Simulations were performed using OVERFLOW[6] version 2.2 on a system of overset structured grids, with grid connectivity generated by PEGASUS version 5.2[7]. Spatial discretization of the Euler terms was done with the third-order HLLC upwind scheme. The time integration scheme employed depended on the nature of the solution. Runs were started with the "steady-state mode" of integration, with simple time stepping. Flows that converged to a steady state solution using this input were considered complete. At higher angles-of-attack, many flows exhibited asymptotic unsteadiness, and these solutions were solved using the "time-accurate mode," with inner iterations inside the outer second-order backward-difference time integration algorithm. Viscous fluxes were computed with second-order central spatial discretization. Solutions were computed with both the Spalart-Allmaras (SA) and SST turbulence models, which were solved with the same discretization accuracy as the mean flow variables.

USM3D was developed at NASA LaRC. It is part of the NASA Tetrahedral Unstructured Software System[8] (TetrUSS), and was used by NASA LaRC for this computational analysis. TetrUSS includes the GridTool model preparation software, the VGRID/POSTGRID volume mesh generation software and the USM3D computational flow solver[9]. The USM3D code uses the tetrahedral cell-centered, finite-volume RANS method. The implicit Gauss-Seidel scheme and the Roe flux difference-splitting scheme and the SA turbulence model were used for all of the flow simulations. The code was run in first-order spatial accuracy until the residual dropped two orders of magnitude and then automatically switched to generate second-order spatially accurate solutions until full convergence. The meshes were made with a boundary layer grid normal to the wall to yield a value of $y^+ = 0.5$.

III. CFD and Wind Tunnel Results

CFD predictions were made for the HWB cruise and landing configurations in free air and in the LaRC 14'x22' and ARC 40'x80' wind tunnels. All of the results presented in this paper are for a freestream Mach number of 0.20. The CFD and wind tunnel data for the cruise configuration are presented first, followed by the landing baseline Krueger configuration in free air and in the 14'x22' wind tunnel. Finally, a landing acoustic Krueger configuration is presented in free air and in the 40'x80' wind tunnel. All of these configurations are described in more detail below.

A. Cruise Configuration

Extensive CFD predictions were made before the first test in the LaRC 14'x22' wind tunnel. Figure 3 shows the HWB cruise configuration test model in the LaRC 14'x22' wind tunnel. The CFD simulations for the 14'x22' wind tunnel tests were made for the HWB in the cruise and landing configurations. Figure 4 through Figure 6 show a comparison of CFD predictions with wind tunnel results for C_L, C_D, and C_M for the cruise configuration and the vehicle in free air. The wind tunnel data in the figures are the fully-corrected data which has been processed to account for the wind tunnel walls using classical wind tunnel wall corrections. These corrections are designed to remove the effects of the wind tunnel walls but do not account for the influence of the sting on the model. For this reason, the CFD results are shown for the configurations with the model and sting in free air. Preliminary data from three wind tunnel runs are plotted to show the range of variation in the experimental data. The final wind tunnel data is pending balance calibration results and is not currently available. The r84 notation for the 14'x22' data stands for run 84. The lower case "r" in the 40'x80' key label stands for a run in the

Figure 3. HWB model cruise configuration in NASA LaRC 14'x22'

January to February 2015 wind tunnel test and the capital "R" stands for a run in the June to August 2015 wind tunnel test. This run notation is used in all of the plots. The predicted results show good agreement with the measured values of lift, drag, and pitching moment up to the stall angle. After the onset of stall there is less agreement between the predicted and measured values.

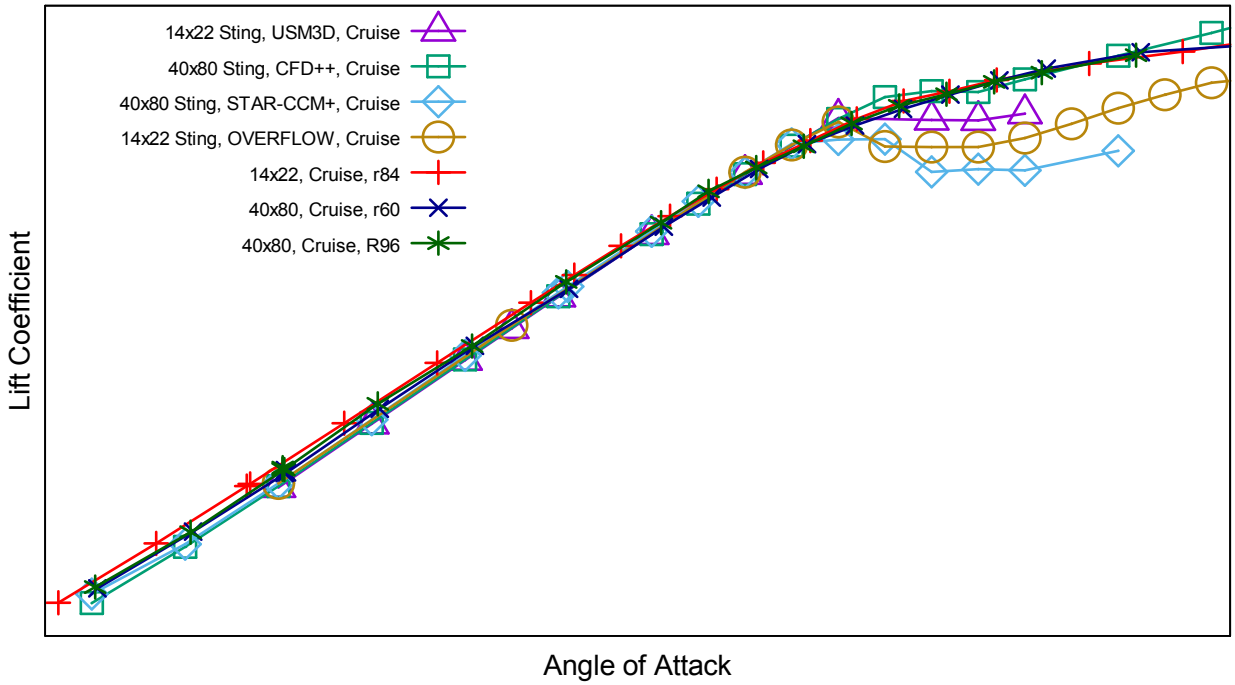

Figure 4. C_L comparisons of the cruise HWB CFD (modeled in free air) with the fully-corrected 14'x22' and 40'x80' wind tunnel data.

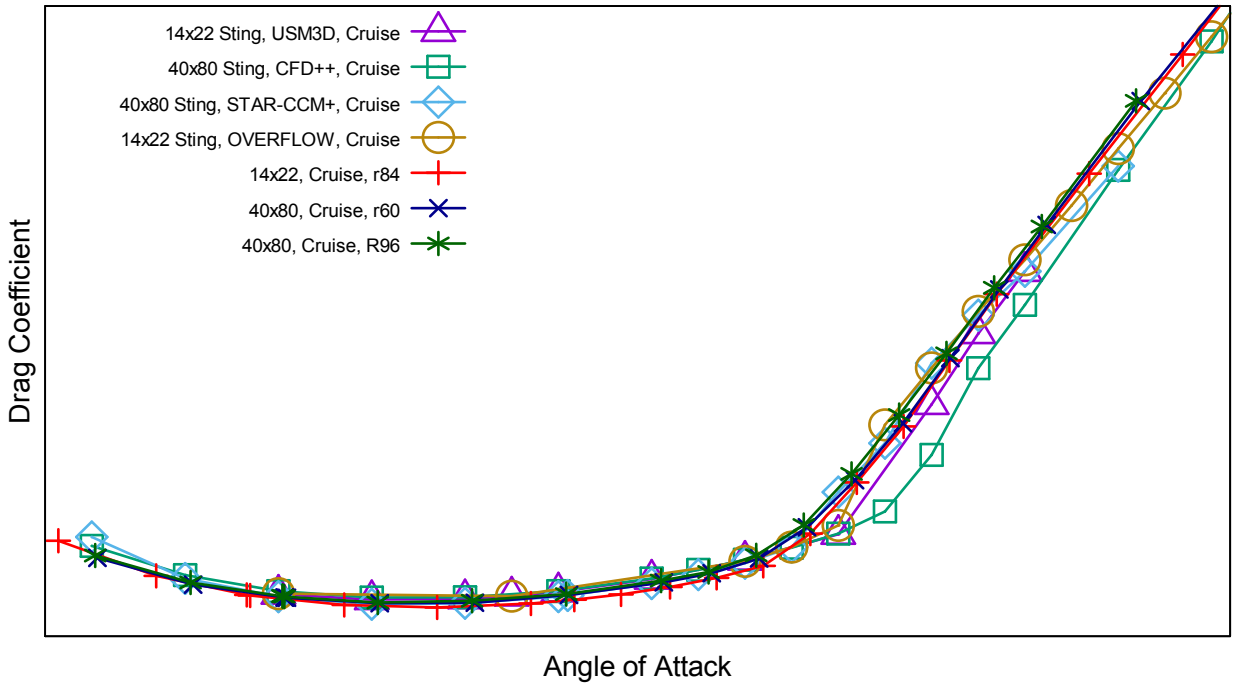

Figure 5. C_D comparisons of the cruise HWB CFD (modeled in free air) with the fully-corrected 14'x22' and 40'x80' wind tunnel data.

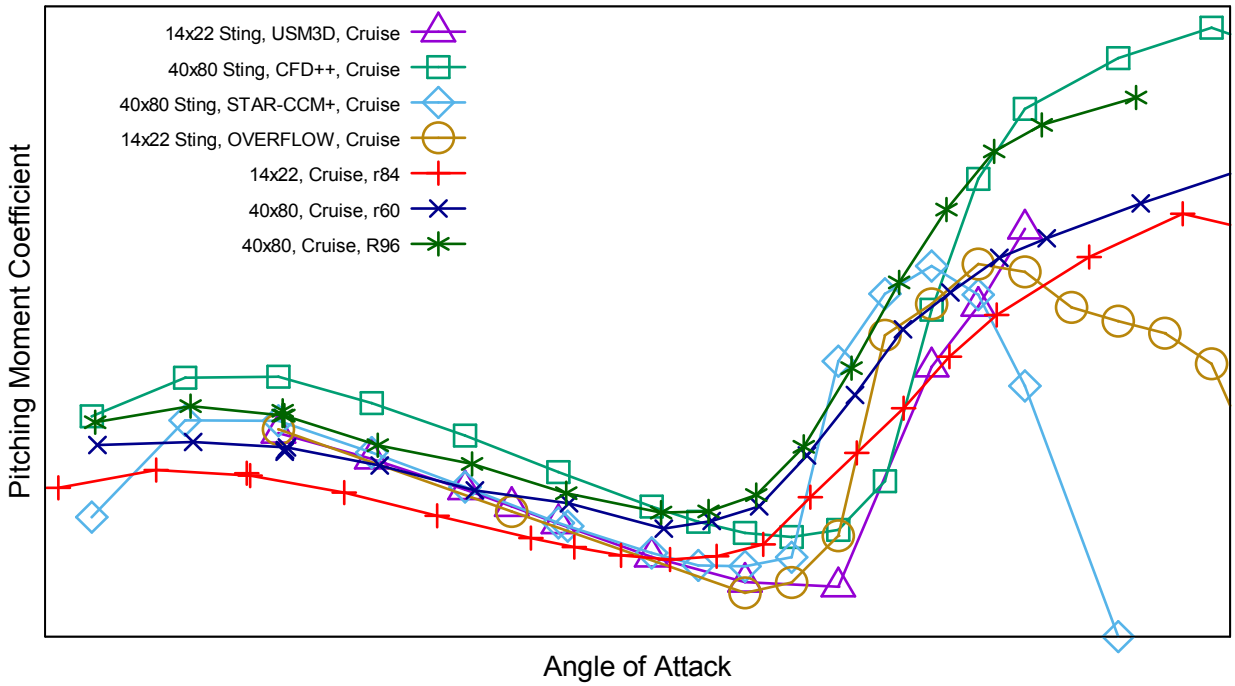

Figure 6. C_M comparisons of the cruise HWB CFD (modeled in free air) with the fully-corrected 14'x22' and 40'x80' wind tunnel data.

B. Landing 45°-2x2 Baseline Krueger Configuration in Free Air

The landing baseline Krueger flap configuration had a smooth underside as shown in Section A-A of Figure 7. After much of the CFD simulation work was completed for the 14'x22' wind tunnel test, the baseline Krueger flap was modified by creating a cutout on the underside of the flap to better represent what is expected on the full scale aircraft and its contribution to the acoustic environment. The modified flap is called the acoustic Krueger flap and is shown in Figure 7 with the baseline Krueger. The acoustic Krueger flap was tested in a matrix of positions and deployment angles in the LaRC 14'x22' wind tunnel to identify the optimal position for maximum lift. Figure 8 shows the matrix of positions for the landing and takeoff configurations and how the deployment angle was specified for the Krueger flap.

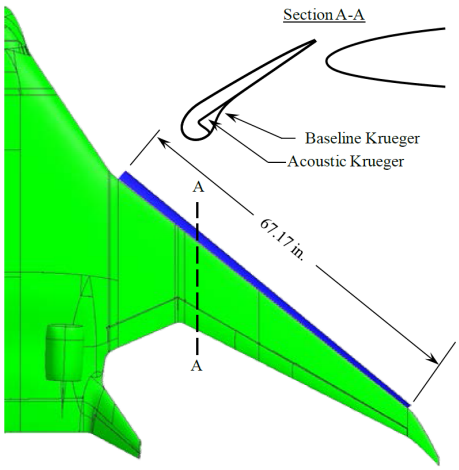

Figure 7. Baseline and Acoustic Kruegers.

The CFD simulations prior to the LaRC 14'x22' foot wind tunnel test were made with the baseline Krueger in the 45°-2x2 position, where the 45° refers to the flap deflection angle and the '2x2' refers to the 'L22' landing Krueger location depicted in the matrix shown on the upper left of Figure 8. One entry was completed in the 14'x22' wind tunnel test with the baseline Krueger in the 45°-2x2 position to provide

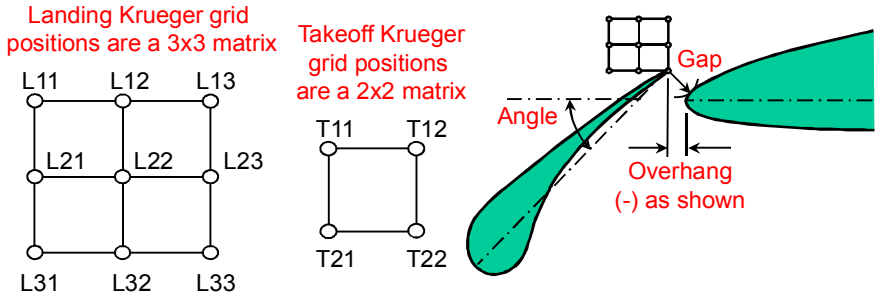

Figure 8. Illustration of Krueger grid positions and angle.

validation data for the CFD codes. Figure 9 through Figure 11 show a comparison of the CFD predictions with the preliminary 14'x22' fully-corrected wind tunnel data for C_L, C_D, and C_M. The CFD predictions included the sting.

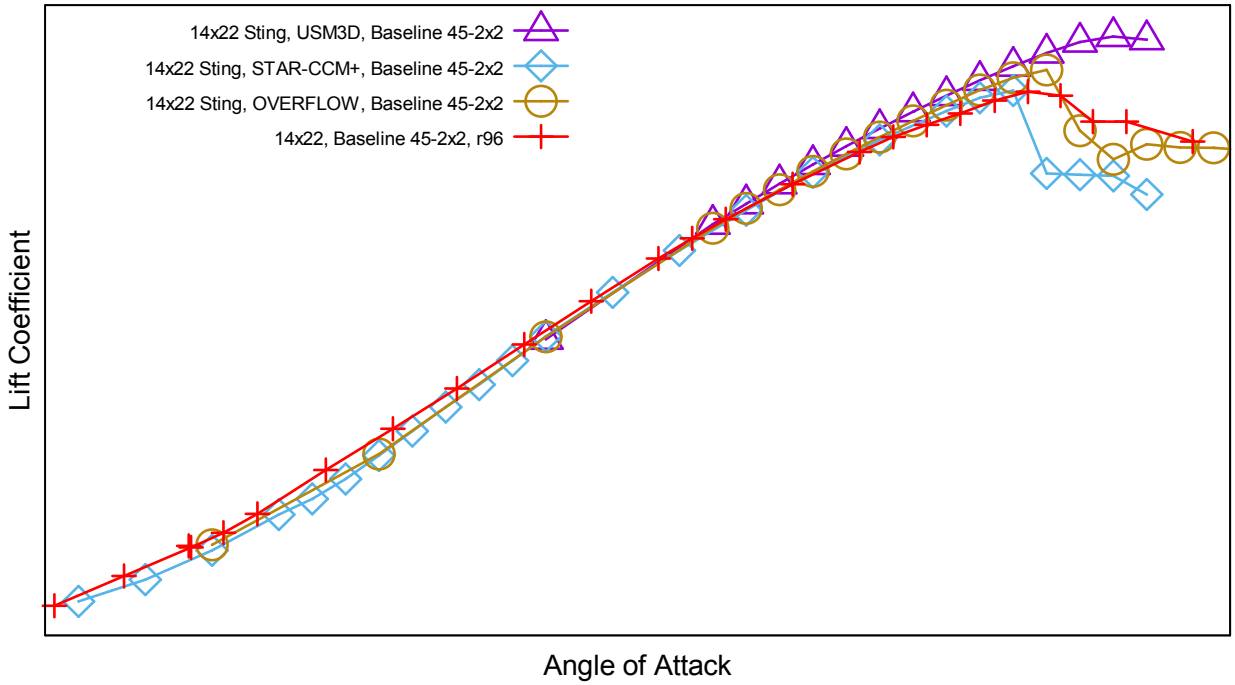

Figure 9. C_L comparisons of the baseline 45°-2x2 Krueger HWB CFD (modeled in free air) with the fully-corrected 14'x22' wind tunnel data.

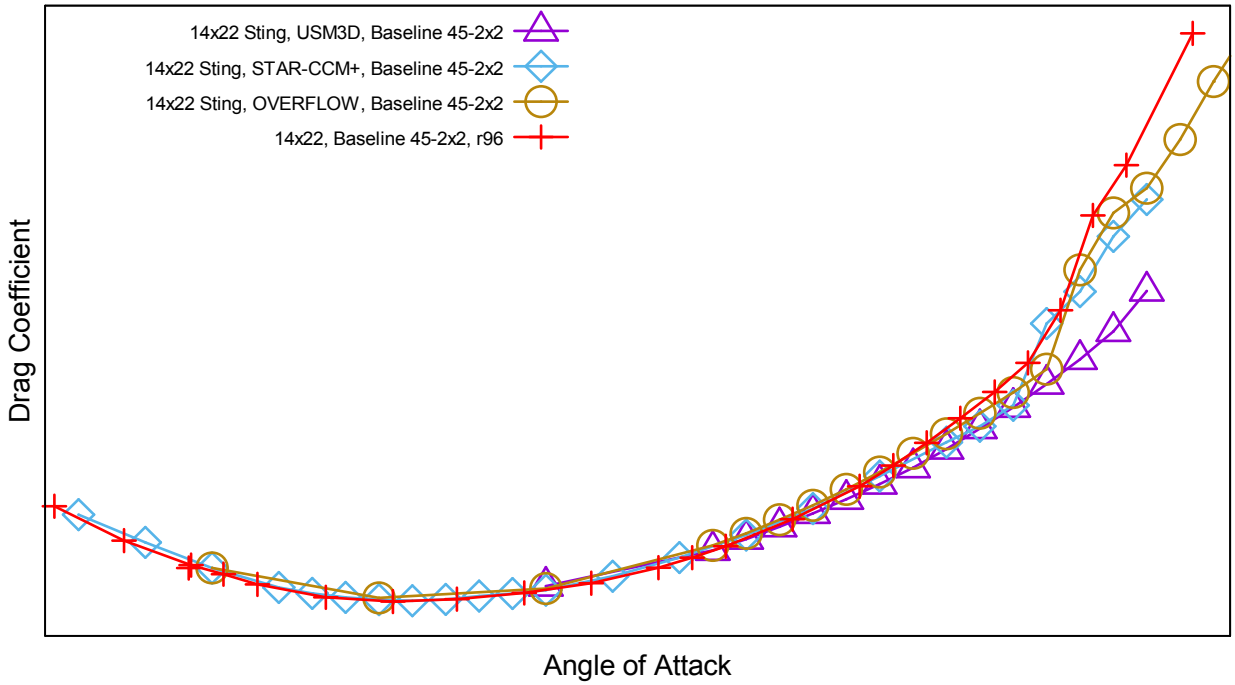

Figure 10. C_D comparisons of the baseline 45°-2x2 Krueger HWB CFD (modeled in free air) with the fully-corrected 14'x22' wind tunnel data.

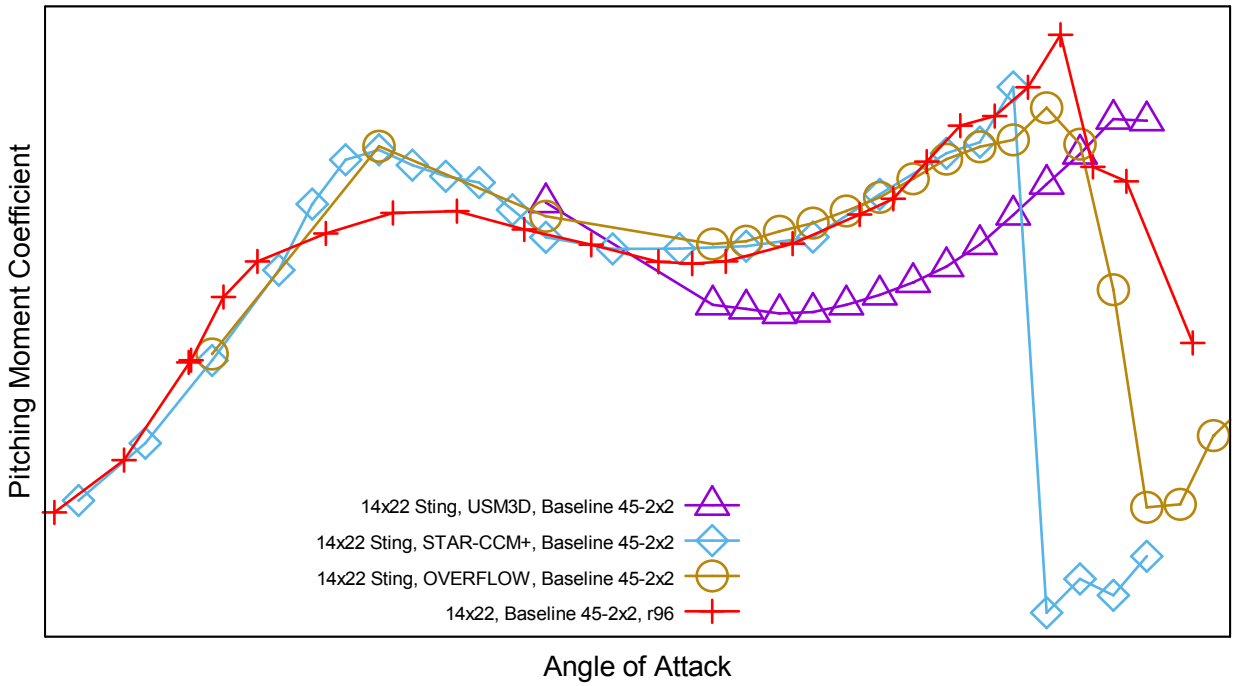

Figure 11. C_M comparisons of the baseline 45°-2x2 Krueger HWB CFD (modeled in free air) with the fully-corrected 14'x22' wind tunnel data.

C. Landing Baseline 45°-2x2 Krueger Configuration in the 14'x22' Wind Tunnel

CFD simulations were computed using two of the codes for the baseline 45° -2x2 Kueger configuration in the 14'x22' wind tunnel. To make the wind tunnel more manageable to simulate, it was modeled with a constant cross section and a slip boundary condition on the wind tunnel walls. The 174" x 261" (14.5'x21.75') cross section shown in Figure 12 was used in the CFD simulations. This is the size of the wind tunnel at the inflow plane of the test section.

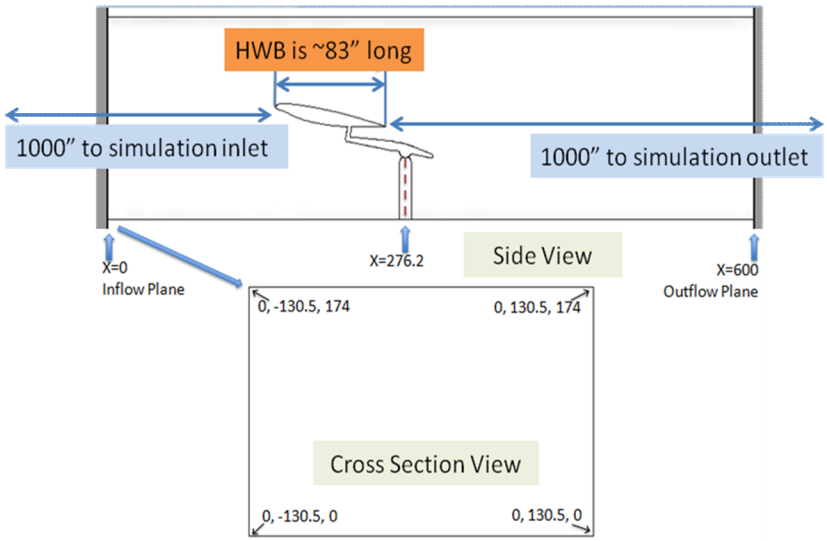

Figure 12. 14'x22' Wind tunnel CFD model.

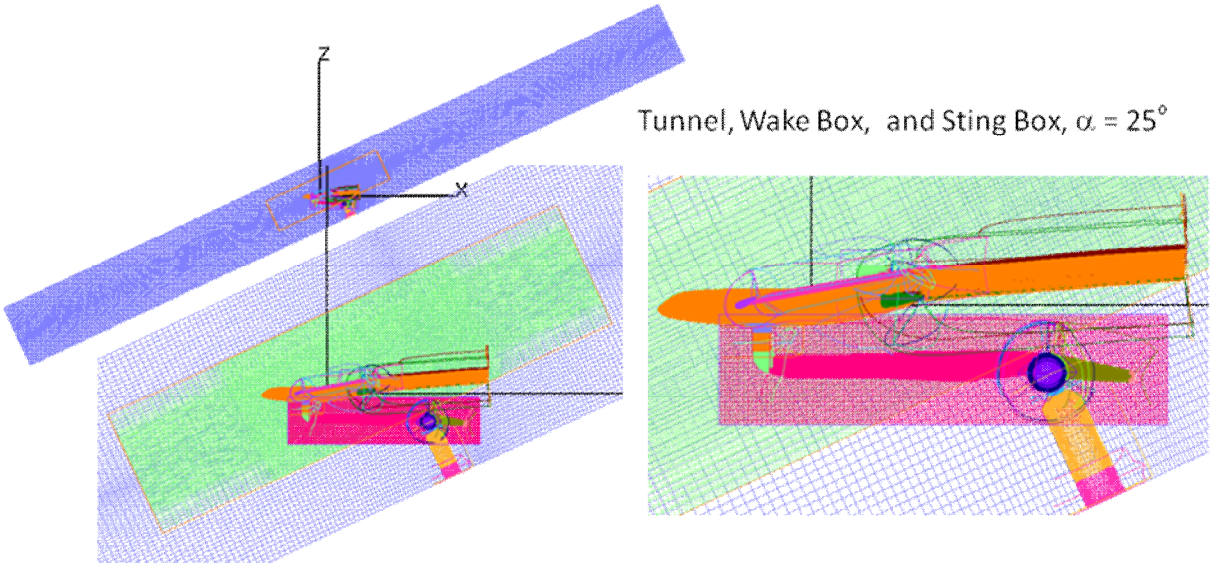

Figure 13. OVERFLOW meshing approach for 14'x22' wind tunnel simulations.

The OVERFLOW simulations modeled the tunnel test section as being twice as long as the 600 inch long test section shown in Figure 12, and the STAR-CCM+ simulations similarly modeled it as extending 1000" fore and aft of the model. The tunnel length was extended in these CFD simulations so as to isolate the HWB model flow from the CFD domain inlet and outlet boundaries. Figure 13 shows the overset meshing strategy used in the OVERFLOW simulations for $\alpha = 25°$. Figure 14 through Figure 16 show the C_L, C_D, and C_M values for the baseline configuration for the CFD codes and the 14'x22' wind tunnel test data. In this case, the wind tunnel uncorrected values are the most appropriate to use when comparing these CFD data to the wind tunnel measurements. The fully-corrected wind tunnel measurements are included to show their variation from the uncorrected values. These figures show that the addition of modeling the wind tunnel walls in the CFD simulations improves the CFD agreement with the experimental data for some angles of attack.

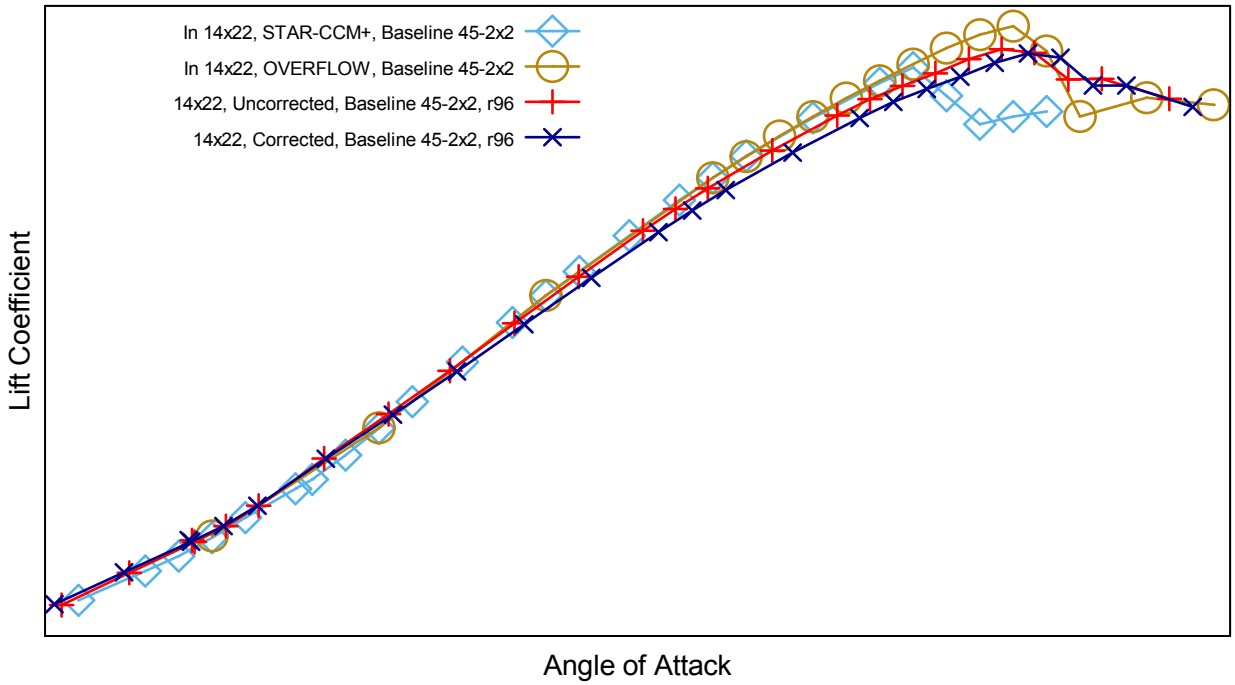

Figure 14. C_L comparisons of the baseline 45°-2x2 Krueger HWB CFD (modeled in the 14'x22' wind tunnel) with the uncorrected and fully-corrected 14'x22' wind tunnel data.

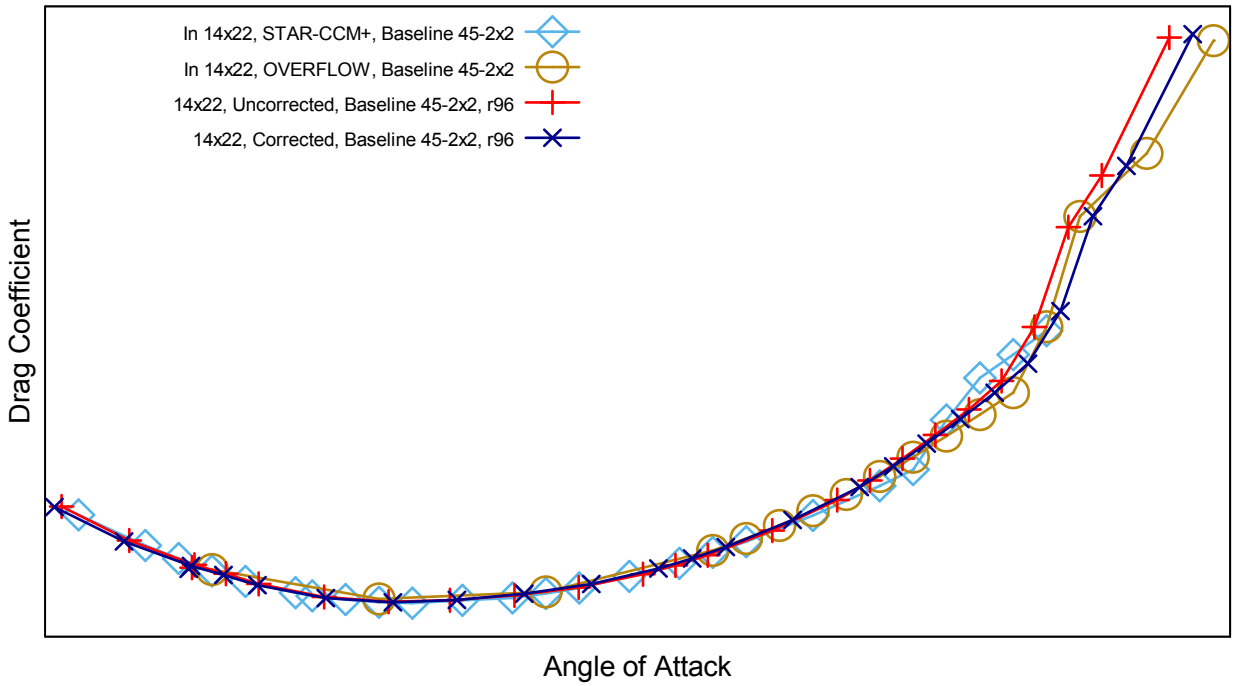

Figure 15. C_D comparisons of the baseline 45°-2x2 Krueger HWB CFD (modeled in the 14'x22' wind tunnel) with the uncorrected and fully-corrected 14'x22' wind tunnel data.

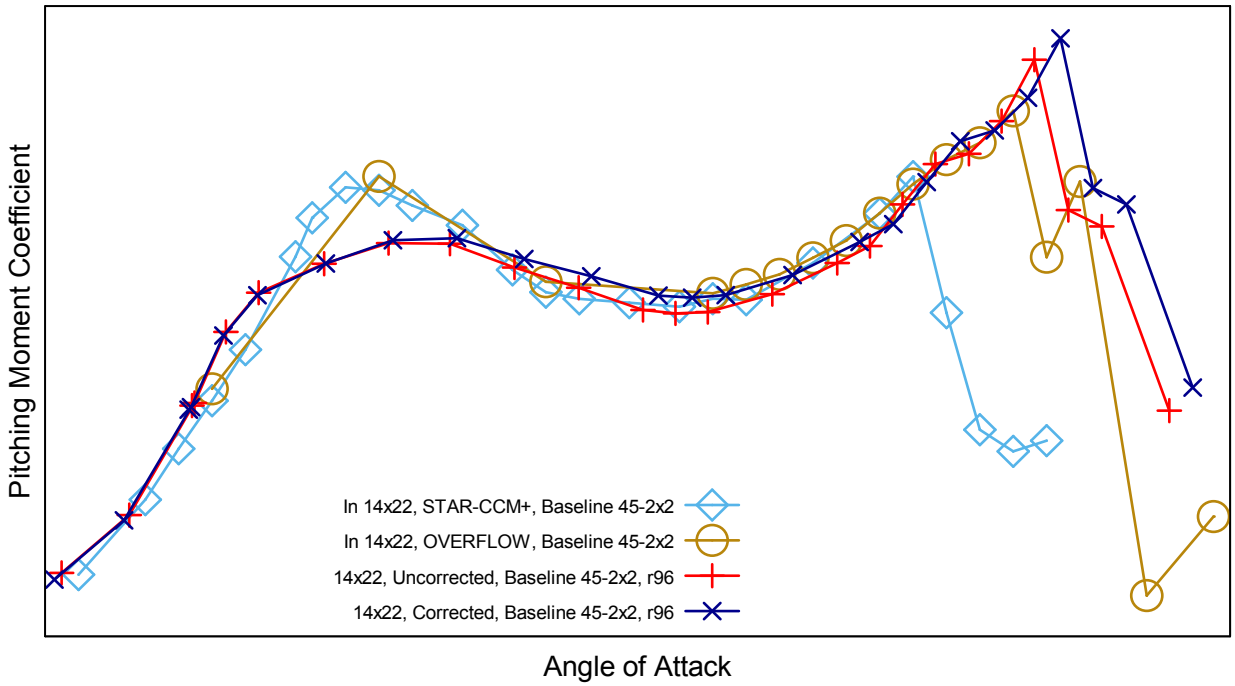

Figure 16. C_M comparisons of the baseline 45°-2x2 Krueger HWB CFD (modeled in the 14'x22' wind tunnel) with the uncorrected and fully-corrected 14'x22' wind tunnel data.

D. Landing Acoustic 45°-3x2 Krueger Configuration in Free Air

After the LaRC 14'x22' wind tunnel testing was complete, the model was tested in the NASA ARC 40'x80' wind tunnel. Figure 17 shows the model installed in the NASA ARC 40'x80' wind tunnel. Large and small acoustic arrays were installed near the tunnel floor to the left of the model. For these tests, the baseline configuration was the acoustic flap in the landing 45^{o}-3x2 position (Figure 8). Three of the CFD codes were used to make simulations for this new configuration. While the 14'x22' wind tunnel CFD simulations were run without the Krueger flap structural brackets, the 40'x80' wind tunnel simulations were run with five structural brackets on each wing. Figure 18 shows a top view of the structural brackets and the 40'x80' wind tunnel sting and vertical support. A bottom view of brackets with a close up of the surface mesh on the center bracket is shown in Figure 19. Figure 20 through Figure 22 show the C_L, C_D, and C_M values for the acoustic configuration for the CFD codes and the 14'x22' and 40'x80' wind tunnel tests. The predicted results again show good agreement with the measured values of lift, and drag up to the stall angle. The pitching moment plot shows slightly larger variation in the different predicted CFD results but for the most part the CFD results follow the same trend as the measured results up to the stall angle. After the onset of stall there is less agreement between the predicted and measured values.

Figure 17. HWB model in the ARC 40'x80' wind tunnel.

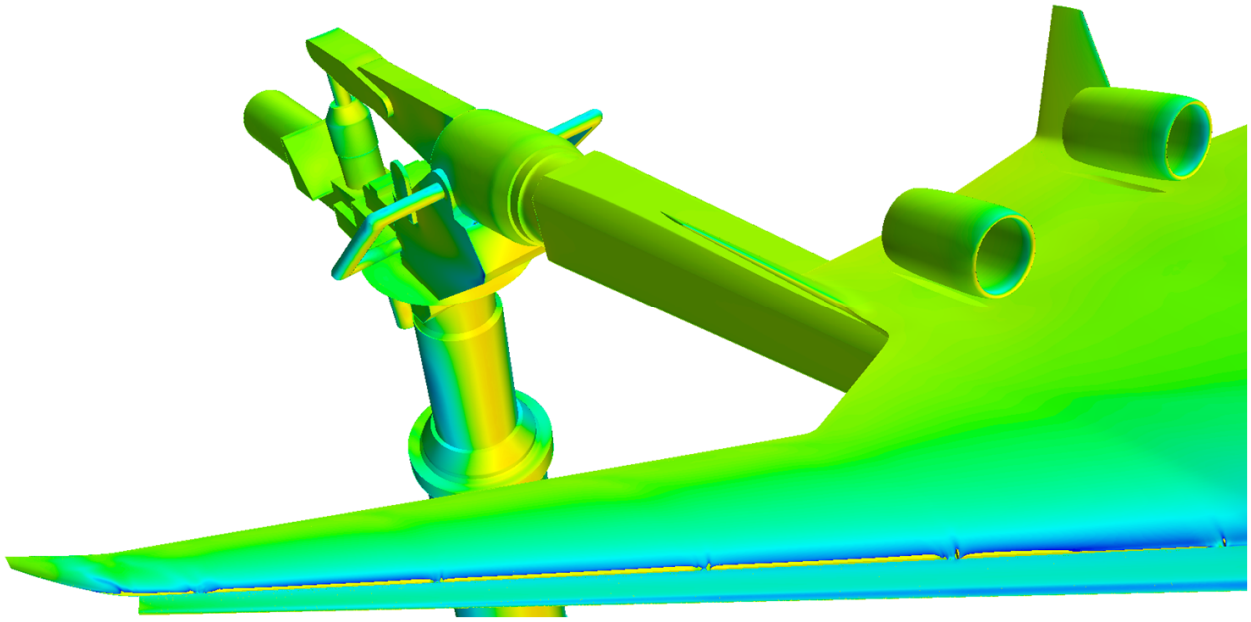

Figure 18. Top view of the right wing pressure distribution showing flap brackets and 40'x80' sting and support.

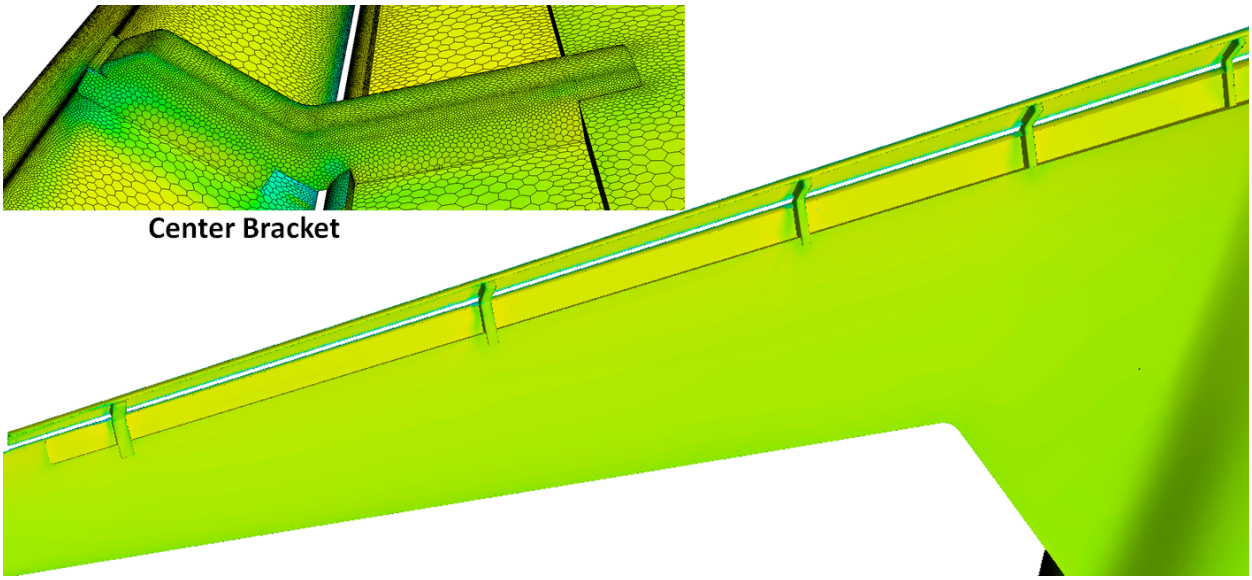

Figure 19. Bottom view of right wing pressure distribution showing flap brackets, acoustic Krueger flap shape, and flap well.

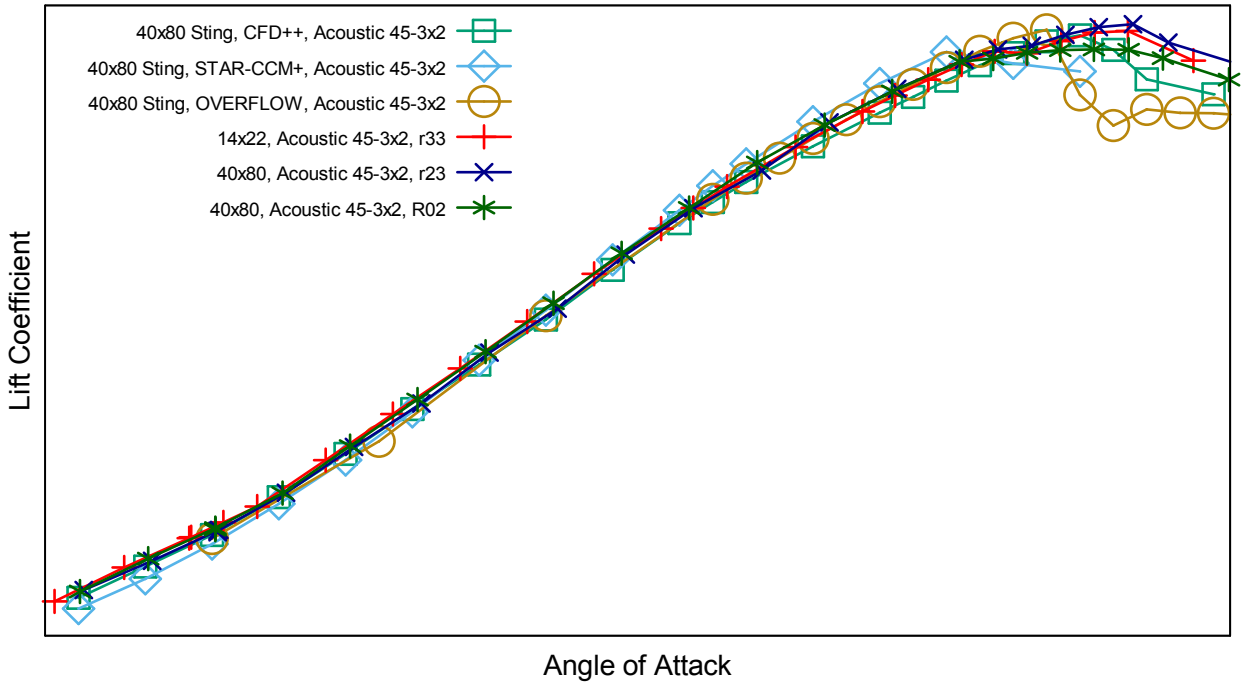

Figure 20. C_L comparisons of the acoustic 45°-3x2 Krueger HWB CFD (modeled in free air) with the fully-corrected 14'x22' and 40'x80' wind tunnels data.

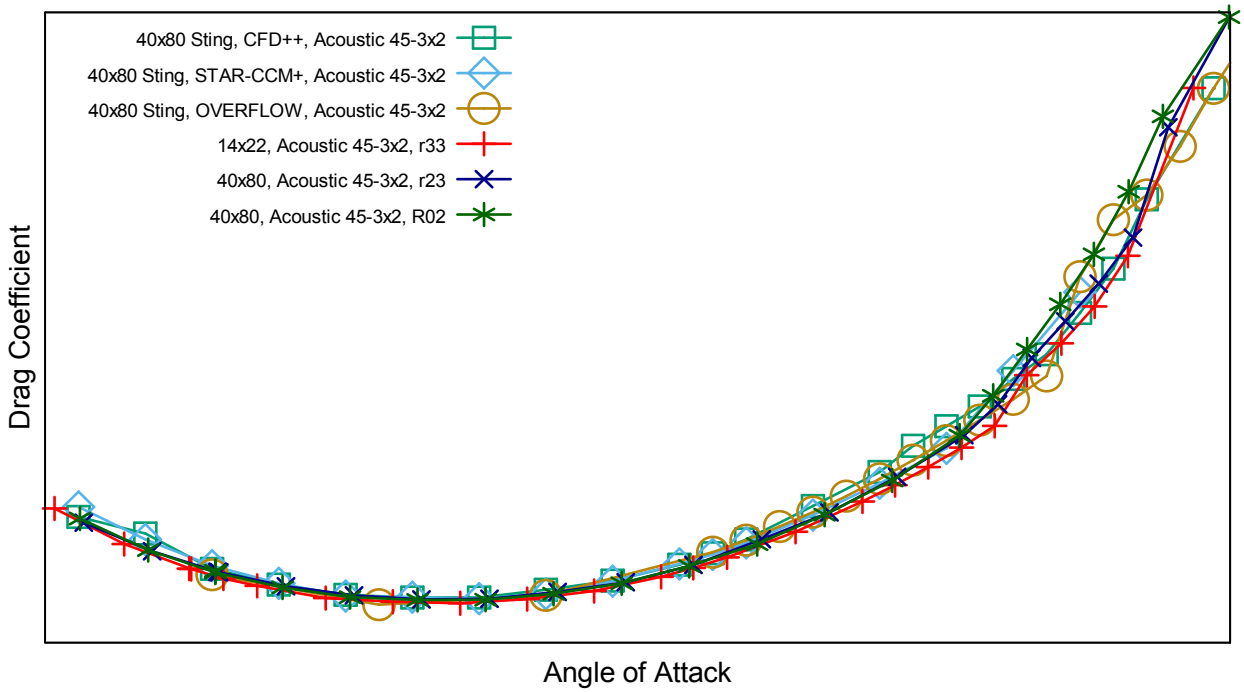

Figure 21. C_D comparisons of the acoustic 45°-3x2 Krueger HWB CFD (modeled in free air) with the fully-corrected 14'x22' and 40'x80' wind tunnels data.

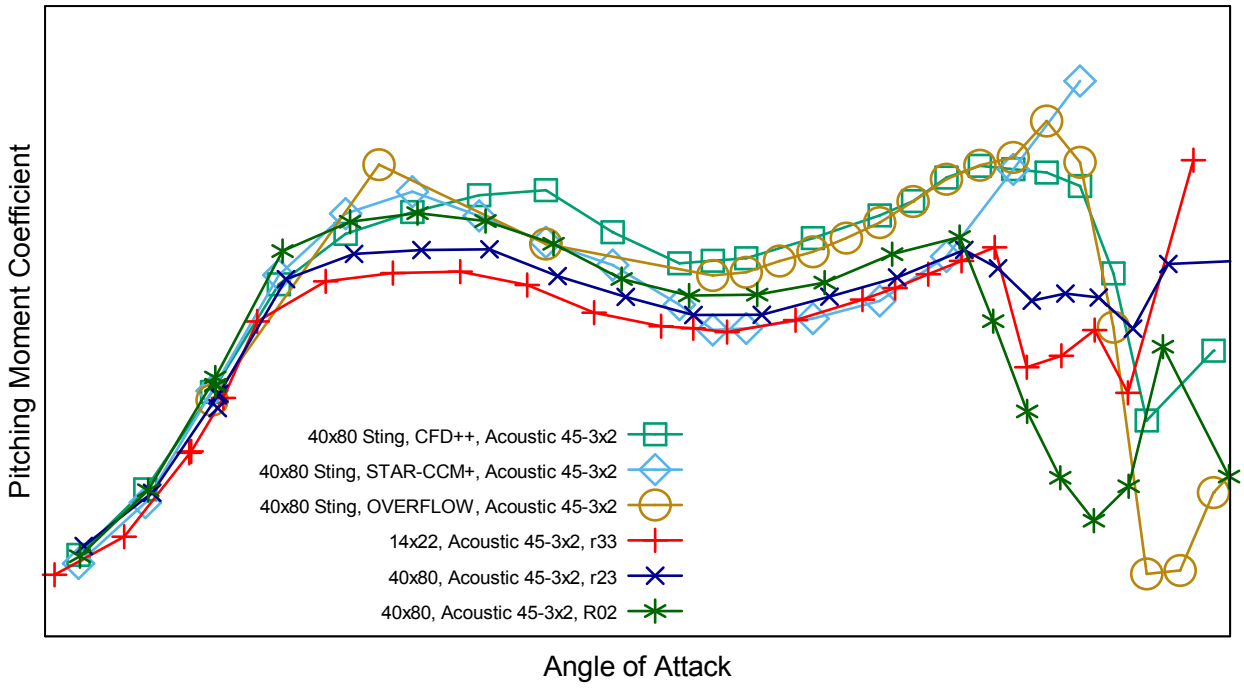

Figure 22. C_M comparisons of the acoustic 45°-3x2 Krueger HWB CFD (modeled in free air) with the fully-corrected 14'x22' and 40'x80' wind tunnels data.

E. Landing Acoustic 45°-3x2 Krueger Configuration in the 40'x80' Wind Tunnel

To investigate the effect of the wind tunnel walls on the measured forces and moments, the HWB was modeled in the ARC 40'x80' wind tunnel with the sting and support post included using the OVERFLOW and STAR-CCM+

codes. For the OVERFLOW simulations, the wind tunnel was modeled with a constant cross section with the size and shape of the 40'x80' wind tunnel test section. Again, a slip wall boundary condition was used for the OVERFLOW wind tunnel walls. This is the same process that was used for modeling the 14'x22' wind tunnel.

For the STAR-CCM+ code, the wind tunnel was modeled from the beginning of the inlet diffuser to the end of the outlet diffuser as shown in Figure 23. The 40'x80' wind tunnel has large vortex generators on the tunnel walls at the beginning of the outlet diffuser. These vortex generators were also included in the STAR-CCM+ simulations as shown in Figure 24. Due to the presence of the 40'x80' wind tunnel in the computational domain, a mesh had to be created for each angle-of-attack modeled. These meshes ranged in size from 120 million to 129 million polyhedral cells. The wind tunnel walls were modeled with a viscous boundary condition.

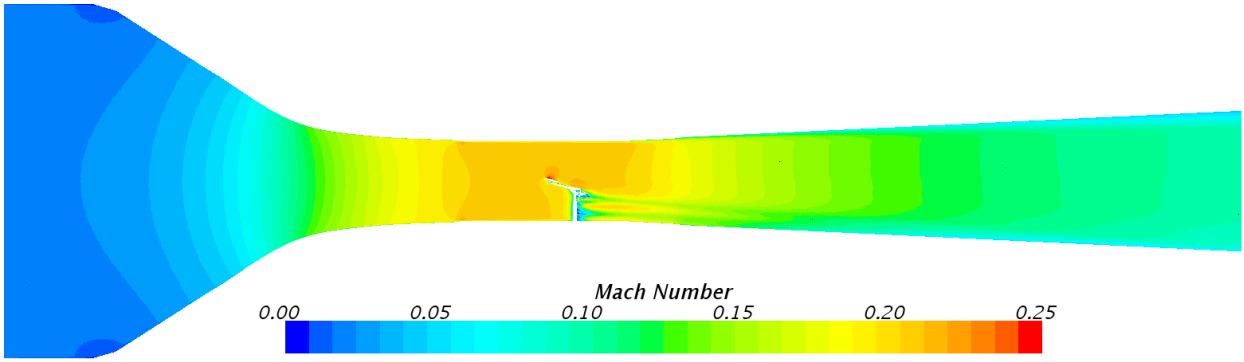

Figure 23. STAR-CCM+ Mach number on symmetry plane for 40'x80' wind tunnel simulation for α = 15°.

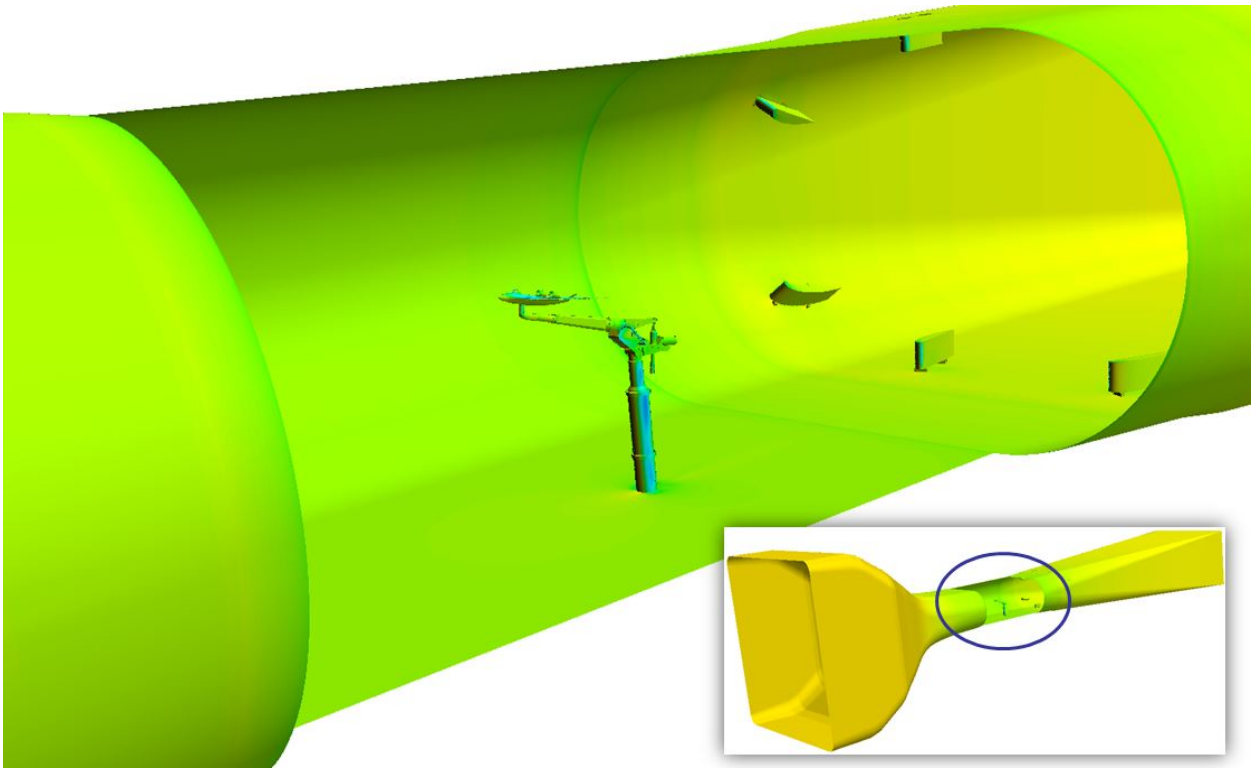

Figure 24. STAR-CCM+ Pressure Coefficient of 40'x80' wind tunnel simulation for α = 15°.

Figure 25 through Figure 27 show the CFD predictions and the preliminary wind tunnel results for C_L, C_D, and C_M for the acoustic Krueger flap with structural brackets in the ARC 40'x80' wind tunnel. The wind tunnel data included in the plots are the uncorrected values that have not been processed to account for the wind tunnel walls or the sting. These figures show an improved agreement between the CFD predictions and the wind tunnel data when the wind tunnel walls are included in the simulations.

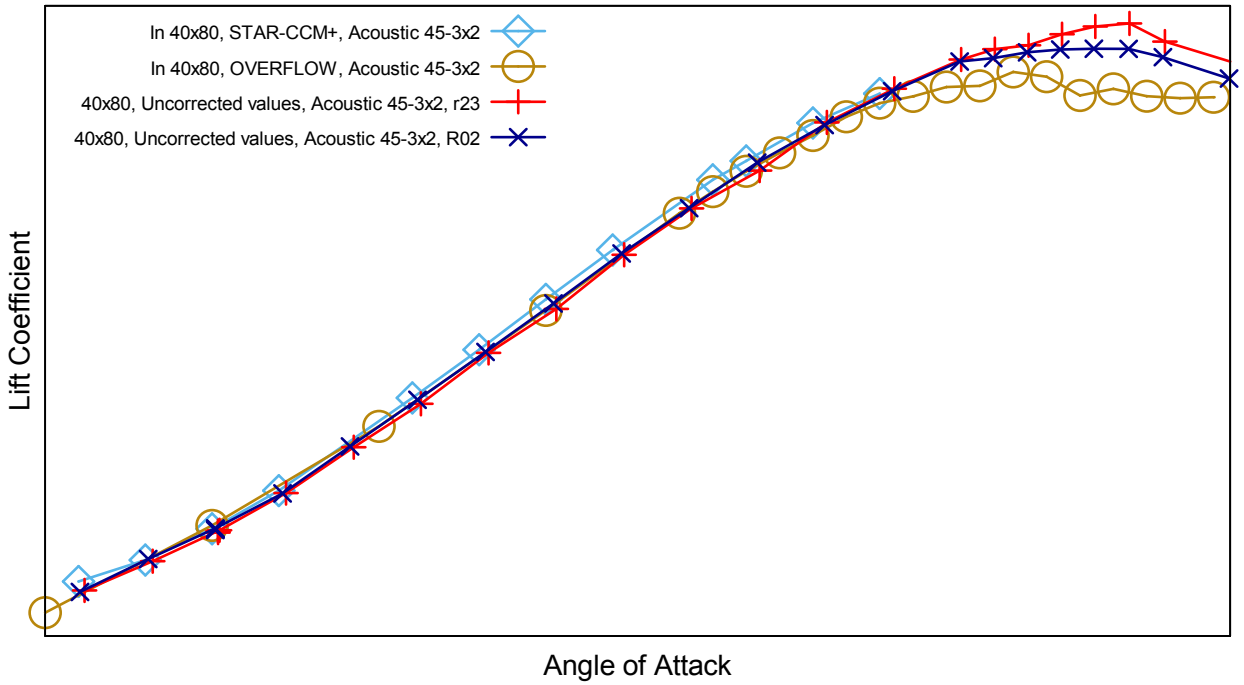

Figure 25. C_L comparisons of the acoustic 45°-3x2 Krueger HWB CFD (modeled in the 40'x80' wind tunnel) with the uncorrected 40'x80' wind tunnel data.

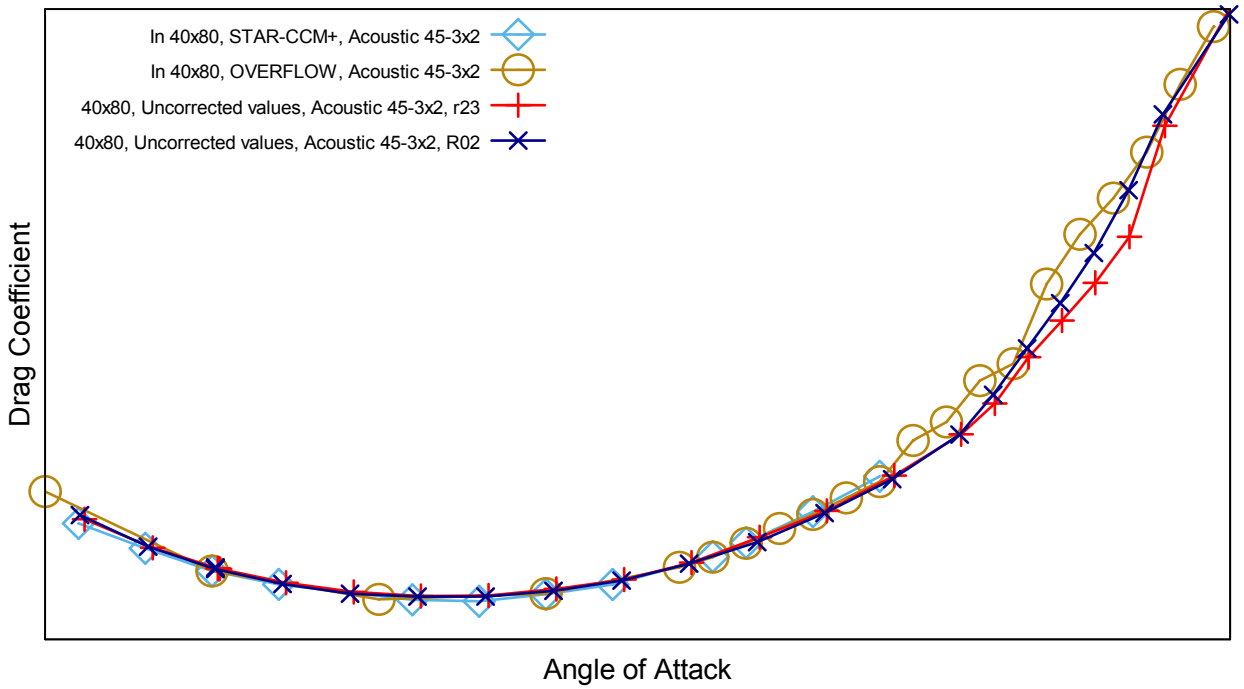

Figure 26. C_D comparisons of the acoustic 45°-3x2 Krueger HWB CFD (modeled in the 40'x80' wind tunnel) with the uncorrected 40'x80' wind tunnel data.

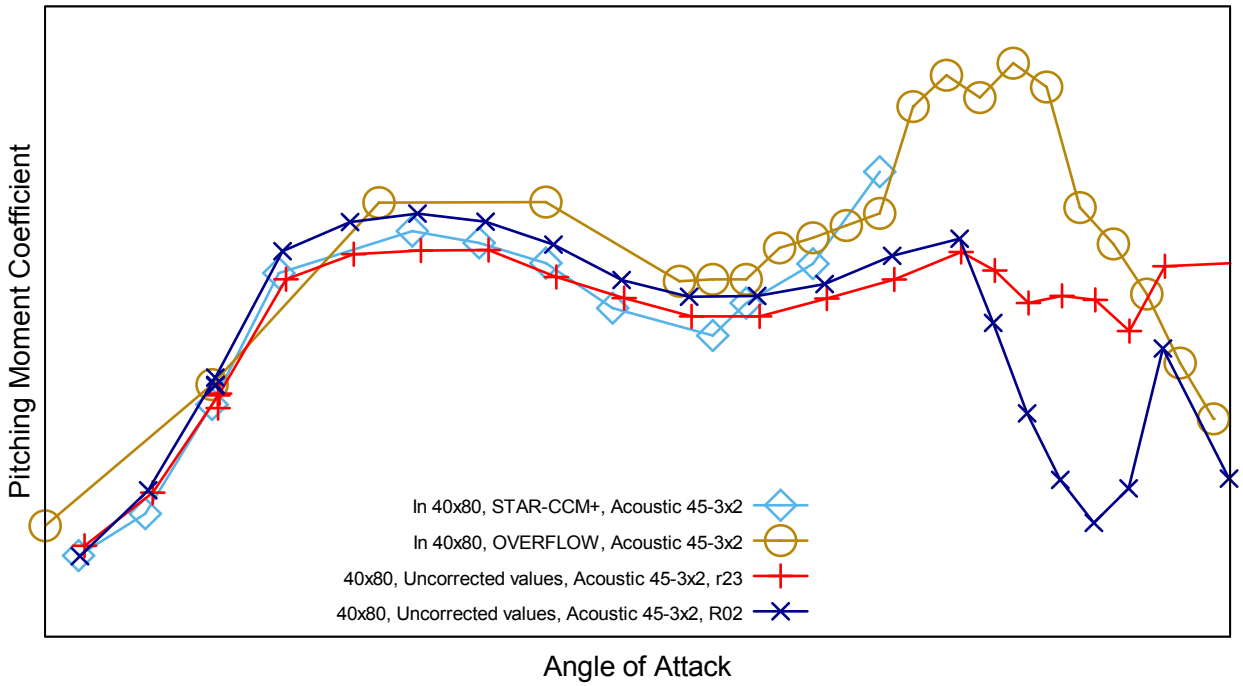

Figure 27. C_M comparisons of the acoustic 45°-3x2 Krueger HWB CFD (modeled in the 40'x80' wind tunnel) with the uncorrected 40'x80' wind tunnel data.

F. Summary of CFD Predictions

Table 1 shows a matrix of the CFD predictions and wind tunnel data included in this report. None of the configurations were run by all of the codes. For the CFD simulations of the HWB in a wind tunnel with the sting and support, the tunnel modeled is listed in the table.

Table 1. Matrix of CFD predictions and wind tunnel results.

	14'x22'	40'x80'	USM3D	CFD++	STAR-CCM+	OVERFLOW
Cruise in Free Air			14'x22' Sting	40'x80' Sting	40'x80' Sting	14'x22' Sting
Cruise in Tunnel	x	x				
Baseline Krueger 45°-2x2 in Free Air			14'x22' Sting		14'x22' Sting	14'x22' Sting
Baseline Krueger 45°-2x2 in Tunnel	x				14'x22' Tunnel	14'x22' Tunnel
Acoustic Krueger 45-3x2 in Free Air				40'x80' Sting	40'x80' Sting	40'x80' Sting
Acoustic Krueger 45-3x2 in Tunnel	x	x			40'x80' Tunnel	40'x80' Tunnel

IV. Conclusion

CFD simulations were performed before and after testing the 5.75% scale model of the Boeing 0009GM HWB in the NASA LaRC 14'x22' and NASA ARC 40'x80' wind tunnels. The results presented show the level of agreement between the results from the two wind tunnel tests and the CFD predictions from four different codes. The predicted results demonstrate good agreement with the measured results up to the stall angle of attack and less agreement after the onset of stall. The predicted results also show that including the tunnel walls in the CFD simulations increases the agreement with the experimental data.

Acknowledgments

The research reported in this paper was sponsored by the NASA Integrated Aviation Systems Research Program's Environmentally Responsible Aviation Project. Computer resources used for the ARC and LaRC CFD predictions in this report were provided by NASA and performed at the NASA Supercomputing System (NAS) facility at ARC.

References

[1] Dickey, E. D., Princen, N. H., Bonet, J. T., and Ige, G. K., "Wind Tunnel Model Design and Fabrication of a 5.75% Scale Blended-Wing-Body Twin Jet Configuration," *AIAA SciTec 2016*, Washington, DC, Jan. 2016.
[2] Metacomp Technologies website, http://MetaCompTech.com [retrieved 30 Oct 2015].
[3] Pointwise Software website, http://Pointwise.com [retrieved 30 Oct 2015].
[4] CD-adapco website, http://CD-adapco.com [retrieved 30 October 2015].
[5] Buning, P. G., NASA OVERFLOW CFD Code website, http://OVERFLOW.LaRC.nasa.gov, [retrieved 30 Oct 2015].
[6] Tramel, R. W., Nichols R. H., and Buning P. G., "Addition of Improved Shock-Capturing Schemes to OVERFLOW 2.1," AIAA-2009-3988.
[7] Suhs, N. E. Rogers, S. E., and Dietz, W. E. "PEGASUS 5: An Automated Pre-processor for Overset-Grid CFD," AIAA Paper 2002-3186, AIAA Fluid Dynamics Conference, June 2002, St. Louis, MO.
[8] Frink, N. T., Tetrahedral Unstructured Software System (TetrUSS) website, http://TetrUSS.LaRC.NASA.Gov [retrieved 30 October 2015].
[9] Pandya, M. J., Abdol-Hamid, K. S., and Frink, N. T., "Enhancement of USM3D Unstructured Flow Solver for High-Speed High-Temperature Shear Flows," AIAA 2009-1329, The 47th AIAA Aerospace Sciences Meeting, January 5-8, 2009.